Ann. Rev. Fluid Mech. 1988. 20 : 421–85

DIGITAL IMAGE PROCESSING IN FLOW VISUALIZATION

Lambertus Hesselink

Departments of Aeronautics/Astronautics and Electrical Engineering, Stanford University, Stanford, California 94305-2186

1. INTRODUCTION

Flow visualization results from the interaction between light and matter. Classical methods such as shadowgraphy, schlieren photography, and interferometry visualize variation in the index of refraction induced by changes in density, pressure, or temperature. Nonuniformities of these physical observables modify the phase of optical waves, rendered visible by free-space propagation (shadowgraphy), optical processing in the back focal plane of a lens (schlieren photography), or interference with a reference wave (interferometry). The classical methods visualize variations of the index of refraction or spatial derivatives thereof integrated along the light path through the fluid. Three-dimensional space is projected onto a plane with the corresponding reduction in degrees of freedom. Except for axial symmetric or two-dimensional flows, spatial structures cannot be recovered from a single image.

Interior detail may be visualized by illuminating the flow with a sheet of light and imaging scattered radiation from variations in particle density or physical observables. Mie scattering is widely used because particles scatter more efficiently than molecules. Rayleigh- and Raman-scattering cross sections are small, necessitating intense laser sources for flow visualization.

Excellent reviews of classical flow-visualization methods have been published, for example, by Merzkirch (1974) and Lauterborn & Vogel (1984) and a beautiful and inspiring collection of pictures by Van Dyke (1982).

0066-4189/88/0115-0421$02.00

These treatments largely concentrate on discussing the qualitative information provided by optical techniques.

Flow visualization traditionally provides guidance to the design of experiments and support for interpretation of local probe measurements. For instance, the discovery by Brown & Roshko (1974) of large-scale structures in a turbulent shear layer using shadowgraphy has had a pronounced influence on modeling, experimental studies, and hardware design. In the past, quantitative image analysis has been largely restricted to interferograms of two-dimensional flows and time-of-flight measurements of gasdynamic phenomena. A notable exception is the work by Uberoi & Kovasznay (1955), who devised an optical processor for measurement of characteristic turbulent length scales in a compressible wake flow using shadowgraphs. By and large, however, flow visualization has been previously applied to qualitative observation and identification of structures in flows.

The quantitative information represented by images is usually expressed in terms of the space-bandwidth product (SBP) and bits. The SBP is defined as the product of the resolution (mm^{-1}) and the physical dimensions (mm) of the image in each direction and for sampled images is equal to the number of pixels (picture elements). The irradiance value at each pixel is quantized in bits or gray levels. A typical photograph recorded on black-and-white film with a resolution of 100 linepairs mm^{-1} (in each direction) and a size of 200×250 mm^2 represents a space-bandwidth product of 5×10^8, or 4×10^9 bits of information assuming 256 quantization levels. This is the equivalent of approximately 200,000 pages of text, making the task of digital image processing computationally intensive and the use of parallel architectures highly desirable.

The human visual system has remarkable processing power in this respect. Structural information in images is easily discerned, and much extraneous detail, such as slow variations in background brightness level, is ignored by the process of lateral inhibition (Pratt 1978). Inference (Marr 1982) is another powerful process by which unknown imagery is compared with previously learned information and structures are identified and classified. On the other hand, making quantitative comparisons between brightness levels in different segments of the image is a difficult task for humans.

The present state-of-the-art in digital image processing is complementary to our visual system. Sampled and quantized images are usually processed on a pixel-by-pixel basis, and quantitative comparisons between pixels are routinely carried out. Global structural identification and classification is more difficult to achieve with present serial processors, and the human visual system obtains superior results compared with those a-

chieved by numerical procedures. Recent work in neural network computing has attempted to mimic brain processing (Paek & Psaltis 1987), but so far promising architectures have not yet yielded tangible results for image processing and recognition.

Classical approaches to image processing have been primarily developed for scene analysis and have been discussed, for example, by Pratt (1978), Castleman (1979), and Andrew & Hunt (1978). In this review, state-of-the-art digital image-processing procedures for flow visualization are discussed and frequent reference to these general textbooks is made, without explicit excitation. In this context, flow visualization is assumed to provide two- or three-dimensional imagery, with the domain of one-dimensional signal processing left to published reviews (Durst et al. 1976). An exception is image synthesis, a technique for assembling images of higher spatial dimension from a time sequence of point, line, or planar data.

Flow-visualization techniques are classified in Figure 1. The chart represents classical experimental methods (shown in italics) in conjunction with recent new approaches based on digital image processing, such as gradient imaging, tomography, and image synthesis. In addition, flow visualization and analysis of numerically generated data are discussed. Regardless of their origin, once the data are available in digital format, the distinction between the different branches disappears and processing proceeds down the path starting with enhancement and ultimately produces graphics representations or quantitative enumeration for comparison and evaluation purposes.

Digital image processing applied to flow visualization is relatively recent and largely motivated by the present emphasis on detecting and classifying large-scale structures in flows. Techniques developed for analysis of scene imagery are frequently useful for flow applications as well, but important differences remain.

Natural scenes and medical images often exhibit structures and features with well-defined boundaries and delineations between image segments of similar brightness or textural content. Flow imagery, on the other hand, tends to show fuzzy boundaries between different regions caused by diffusion. Edge-detection techniques developed for scene analysis may not be directly useful for flow visualization. Approaches optimized for processing of scalar images are generally inapplicable to vectorial data such as velocity or vorticity fields. However, decomposition of vectors into constitutive elements may bridge the gap between image processing of vectorial and scalar data. In one approach, vector fields are decomposed into two or three scalar components, one image for each component of the field. Each image, representing one vector component, is processed

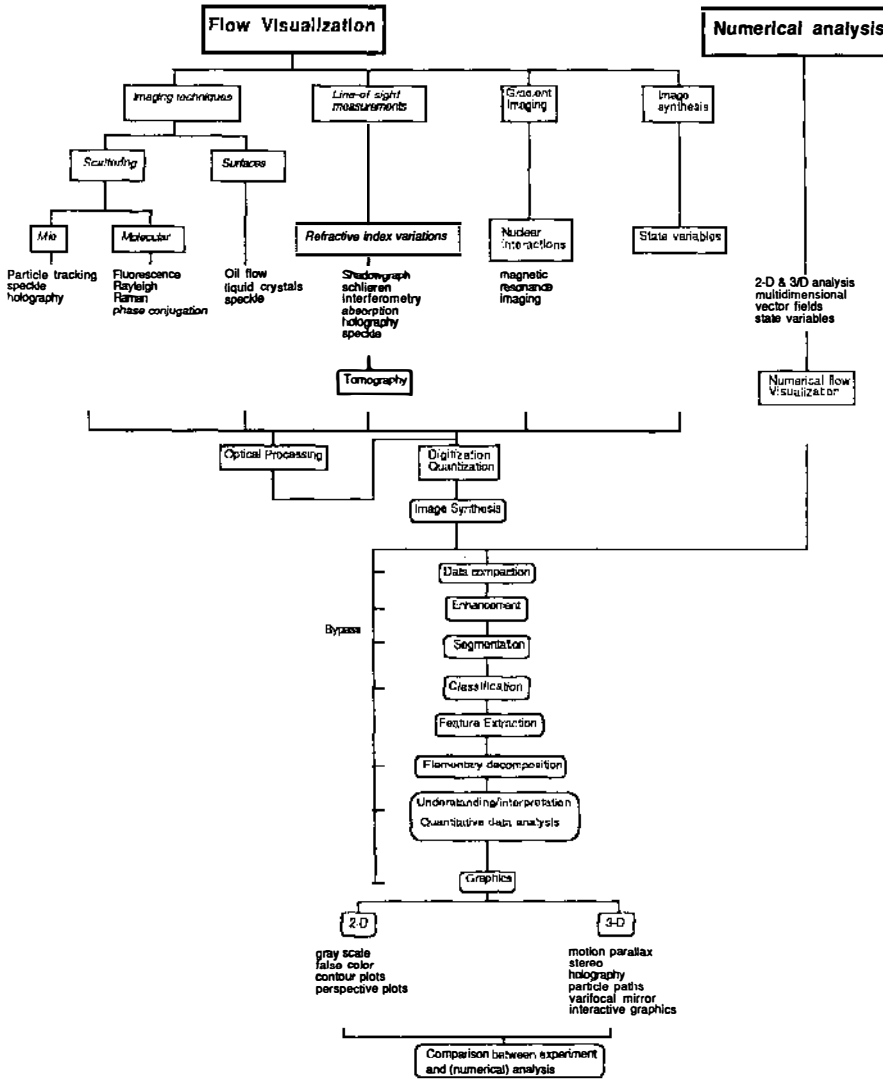

Figure 1 Classification of digital image-processing and flow-visualization techniques.

using conventional methods. The final image is reconstructed by combining the three constitutive images. Another method is based on graph theory and critical-point analysis. The image is decomposed into regions bounded by dividing streamlines connected through nodes or critical points. These local features form a basis for global representation of

flow topology. The topology is reduced to a graph, with the structures represented as the nodes and their relationships in the flow as the connecting lines of the graph. Since the number of different features is limited, substantial data compaction occurs. Yet the information is rich enough to fully characterize the flow, making this representation particularly useful for data-set comparisons. For the approach to have merit for evaluation of large data bases, automated feature extraction is desirable.

The specifics of image analysis depend on the optical imaging configuration used for image acquisition. Underlying physical and optical principles of the various techniques shown in Figure 1 determine to a large extent the required processing steps for extraction of useful image data. Description of the imaging modalities in terms of Fourier optics is particularly valuable, because this linear-systems approach is directly compatible with the theoretical framework describing digital image processing. Indeed, the close relationship between digital and optical processing suggests hybrid approaches for flow visualization. Hybrid processing in its most effective form incorporates the high-speed parallel approach of optical processing and the high-precision capabilities of digital processing. An example of such an approach is the optical processing of double-exposed speckle patterns for determination of velocity fields (Hesselink 1987a). Coupling between optical and digital processing not only enhances classical flow-visualization techniques, but also leads to fundamentally new imaging modalities. For example, the interior detail of a flow is revealed by tomographic processing of schlieren, shadowgraph, or interferometry images recorded at multiple viewing orientations. Digital image processing extends the domain of application of line-of-sight optical techniques to include measurement of space-resolved features. It also allows image representation with resolution orders of magnitude smaller than the wavelength of the probe radiation. In magnetic resonance imaging the flow is subjected to a spatially varying radio-frequency signal that interacts with nuclear spins to produce a response signal suitable for tomographic image reconstruction (Macovski 1983), a technique known as gradient imaging. Resolution is not determined by the wavelength of the probe radiation (on the order of a meter) but by the uniformity of the gradient of the magnetic field. Practical systems now provide submillimeter spatial resolution. This technique provides a powerful new imaging modality for flow visualization in opaque and curved pipes without requiring optical access.

The quality of the images obtained with these new modalities as well as with classical flow-visualization approaches depends to a large extent on consideration given to imaging, sampling, and quantization steps. Since these steps precede any digital processing and are generic to all sections of this review, they are discussed first.

1.1 *Linear-Systems Approach to Imaging and Processing*

Consider a simple imaging configuration in which an object emits or scatters radiation, collected and imaged by a lens onto a recording medium. If the object is infinitesimally small, diffraction blurs the image to a small spot, known as the optical impulse response. On a global scale, the output (or recorded) image is the convolution of the input image and the optical impulse response, assuming space invariance. This configuration is modeled using Fourier optics and linear-systems theory. The components of the block diagram shown in Figure 2 include modeling of the scattering processes, image recording, image sampling, quantization, processing, and display. Each block has associated with it an impulse response or transfer function, and the output image is related to the input via a convolution operation.

Consideration of imaging steps is a prerequisite for accurate digital processing because it is well known that radiometric errors in the digitized data can give rise to large errors in the computed results when proper care is not exercised (Hesselink & White 1983, Jiménez 1984). In this model it is assumed that noise is linearly added to the signal, a condition not always true in practice. Film noise, for instance, is often signal dependent, and accurate modeling requires cepstrum techniques (Oppenheim & Schafer 1975).

Processing of flow-visualization images represented by two-dimensional matrices of gray levels frequently proceeds using matrix–matrix convolution operations. The input image is convolved with a small 3×3 matrix or mask representing the impulse response of the desired operation, producing an enhanced or otherwise modified image. Mask design is well developed and is not discussed here. Operations such as edge enhancement, line detection, and filtering can all be carried out by convolution operations.

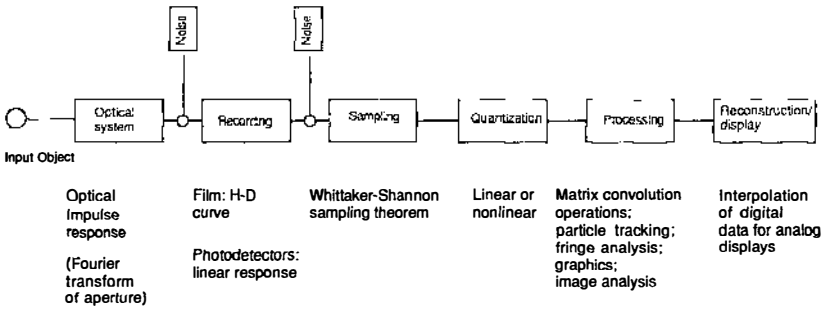

Figure 2 Block diagram of linear image-processing steps.

2. SCATTERING

Scattering techniques rely on interaction between radiation and molecules or seed particles. Three distinct approaches are discussed in this section, namely particle-imaging velocimetry (PIV), laser speckle velocimetry (LSV) and laser-induced fluorescence (LIF). Prior to discussing individual techniques, we first consider a generic scattering configuration.

2.1 *Generic Scattering Configuration*

A sheet of light, derived from a laser, illuminates a section of the flow and scattered radiation is collected and imaged onto detectors or film, as shown in Figure 3. Mie scattering of seed particles is most efficient, and depending on particle size it can be 24 orders of magnitude more intense than vibrational Raman scattering (Goulard 1976). The laser-beam size and intensity vary spatially (a collimated Gaussian beam spreads as a result of refraction), and the scattered light intensity is not uniform from position to position, even for homogeneous seeding.

The optical collection system determines the resolution cell—the smallest area that can be distinguished in the image. In Mie-scattering experiments the seed-particle size is usually smaller than the sheet thickness and can be either larger (PIV) or smaller (LSV) than the resolution cell. From an optics point of view these regimes are distinctly different (Adrian 1986) and lead to varying image-processing approaches.

The distinction between PIV (using a low density of seed particles) and LSV (using large particle density) is more than a formal one. In LSV, density is usually so large that the velocity vector can be obtained on a regular grid of points, whereas in PIV one only obtains a measurement at those locations where particles happen to be during exposure, resulting in a random sampling of the velocity field. To obtain velocity gradients or

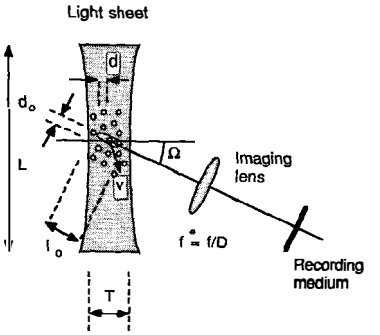

Figure 3 Genetic scattering configuration. The resolution cell has dimensions $d_0 \times l_0$, the sheet thickness is T, the Rayleigh range is L, and the f-number of the lens is f/D.

otherwise process the data, it is frequently necessary to compute the velocity field on a regularly spaced grid. This requires interpolation of randomly spaced data, a process difficult to carry out with high precision. No such interpolation is usually needed for processing of speckle images.

The tacit assumption in these techniques is that the seed particles follow the fluid without significant lag and do not alter the flow dynamics. The first requirement limits the size of particles that can be used to track fluid motion of a certain scale and tends to favor the use of small particles. On the other hand, scattering efficiency is strongly dependent on particle size and concentration; larger and more numerous particles scatter light more efficiently, thereby reducing the required source intensity compatible with a particular recording medium. Trade-off considerations of this kind have been discussed by Adrian (1986) and Sommerscales (1981).

2.2 *Particle-Imaging Velocimetry*

In particle-imaging velocimetry, seeding density is low and individual particles are imaged either as a function of time (particle-streak velocimetry) or in a superimposed sequence of exposures short enough to freeze particle motion.

In principle, particle tracking is straightforward using the steps indicated in Figure 4, but in practice accuracy, resolution, sensitivity, cost effectiveness, and specificity require sophisticated processing techniques. The method involves imaging of the flow on a suitable material, usually film, followed by sampling and quantization, identification of particles, and determination of tracks from which the velocity is computed. Major diffi-

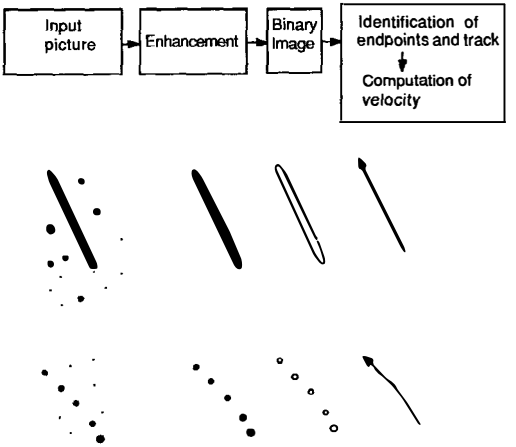

Figure 4 Two examples of particle tracking.

culties arise because particles are indistinguishable from each other unless special precautions are taken using illumination coding. Tracks can also cross, presenting a challenge for automated image analysis. Furthermore, fast particles moving out of the sheet are difficult to distinguish from slower ones staying inside the illumination region.

To circumvent some of these difficulties elaborate illumination codes are used. The light source is flashed several times in a coded sequence to provide multiple images along particle tracks, or alternatively fluorescence is incorporated to mark the tail or head of a particle streak. Color is also useful as a discriminating agent, but its use substantially increases the data-processing burden.

Under the assumption that accurate quantitative data are desired, radiometric corrections need to be made to images recorded on film prior to applying image-processing techniques to the data. Photographic recording is a highly nonlinear process, and errors in the pixel values directly translate into errors in particle location. These considerations are especially important when gradients of the velocity field are desired. In this case it is estimated that the relative error in the velocity needs to be less than 0.5% in order to allow accurate determination of vorticity.

A first step in image processing is often edge detection. The original gray-scale image, in which the pixel value represents the sampled and quantized image irradiance, is reduced to a binary image in which pixel values are either black or white. For this purpose, various approaches are available.

Threshold analysis is a method by which the local pixel value is compared with a predetermined scalar. Larger pixel values are retained and considered part of the particle image, and values smaller than or equal to the threshold are discarded as background. Clearly, when the center of the image is brighter than the edges, the particular choice of threshold may have profound influence on the size of the detected object. Nonuniform background illumination makes application of global thresholding techniques inaccurate, and adaptive approaches are preferred. Some of the ambiguity related to choosing a threshold value is avoided by relying on statistical image analysis and histograms. For example, a bright particle image in a dark background produces a bimodal irradiance histogram. The optimum threshold in this case lies between the peaks.

Other edge-detection techniques include image convolution with a small mask to extract edges of a particular orientation, such as those aligned with the horizontal, 45°, or vertical direction, or with the Sobel or gradient operators, which detect edges isotropically.

From edge information and from knowledge of the end and intermediate points, traces may be uniquely identified by interpolation or morphological

image processing. For example, track-following algorithms look for neighboring pixels in a direction determined by search procedures designed to find local maxima or minima in pixel values. The collection of extrema specifies track length, from which the local velocity is computed through division of track length by the known exposure time.

Complications arise when tracks cross, requiring specific logic for dealing with this problem. Automated procedures are frequently based on finding the most likely direction for the particle path for knowledge of tangents to the already established portion of the track or by analyzing the illumination code patterns within each track. Semiautomatic approaches usually require operator assistance. Alternatively, cross-correlation techniques allow velocity determination without regard to track crossing (Kimura & Takamori 1986).

A major problem in edge detection is noise. Noise contamination produces false results, and automatic feature-extraction programs either rely on a priori information about the noise in order to reduce its effects or incorporate edge-preserving noise-reduction techniques. From the binary or edge image the centroid or other descriptive information, such as the perimeter, surface area, or shape factor, is readily computed. A particularly useful technique for this purpose is morphological image processing because the underlying mathematical framework is optimized for logical operations such as automated skeletonization, region growing, and shrinking (Serra 1982).

2.2.1 APPROACHES TO PARTICLE TRACKING Particle tracking is successfully applied to velocity measurements in internal-combustion engines (Kent & Eaton 1982), to the determination of position, size, shape, and orientation of microscopic particles moving in three-dimensional space (Payne et al. 1984), and to studies of fast-moving gas bubbles in liquids using digital three-dimensional processing of holographic reconstructions (Haussmann & Lauterborn 1980).

The mode of image recording to a large extent determines the particulars of the optimum processing procedure. When the particle moves over a distance more than its own size during the exposure sequence and the density of particles is not very large, tracking is most appropriate. On the other hand, when a double-exposure photograph of a uniformly seeded flow is recorded in such a short period that the particles do not move significantly, optical readout techniques are advantageous for determination of the local velocity vector. Multiple recording with long exposure times of densely seeded flows appears to be an interesting way of relaxing the requirement for intense illumination sources, and argon lasers have been used to achieve good results (Lourenco 1986).

Densely seeded flows are analyzed using optical readout techniques. These involve illumination of the double-exposure negative with a small probe beam, producing Young's fringes in the back focal plane of a lens. The orientation of the fringes is perpendicular to the local velocity vector, and the magnitude of the vector is inversely proportional to the fringe spacing. The fringes are straight and always contaminated with noise. Variations on this technique are discussed in the section on speckle.

Applications of particle tracking to fluid flows are varied and numerous. Dimotakis et al. (1981) reported on particle-streak photography in a plane mixing layer, Marko & Rimai (1985) measured the velocity in the wake of a circular cylinder, Chang et al. (1984) and Marko & Rimai (1985) tracked individual particles, and Gharib et al. (1985) used afterglow of phosphorescent particles to determine velocity vectors. Rimai & Marko (1982) incorporated pulse-code modulation, and Jian & Schmitt (1982) determined water currents by fitting ellipses to short streaks.

2.2.2 ACCURACY CONSIDERATIONS The accuracy of particle-tracking methods depends strongly on the care exercised during recording and image processing and on flow and seeding parameters. In a recent paper, Agui & Jiménez (1987) discussed performance of particle tracking with particular emphasis on error analysis associated with the interpolation of data available at randomly sampled locations. In their work, velocity vectors are determined with sufficient accuracy to warrant computation of vorticity. This is one of the few studies in which results from particle tracking are compared with laser Doppler velocimetry measurements. Imaichi & Ohmi (1983) and Utami & Ueno (1987) also reported vorticity measurements derived from particle tracing, but the manual data-reduction scheme used in the latter study appears to be too inaccurate to produce reliable derivative data. These and other accuracy considerations have been investigated by Chang et al. (1984) and Kobayashi et al. (1986).

2.2.3 EVALUATION The various approaches to particle tracking have not been sufficiently well developed yet to allow a careful comparison between techniques. As a general conclusion, however, it appears that most researchers agree that noise and nonuniform background illumination gradients should be removed prior to performing edge detection and measurement of particle position. In this regard, median filtering is very effective in removing isolated noise spikes. The background uniformity may be improved by decomposing the image into triangle functions and high pass filtering. After an improved image has been obtained, automated procedures such as the gradient and Sobel operators produce results of comparable accuracy, as can be obtained with thresholding, provided a local threshold is used; global thresholding should be avoided unless the

background intensity level is very uniform. If, in addition, the image histogram is a bimodal distribution, optimal thresholding techniques based on histogram statistics should be used for segmentation. In case the background illumination is not uniform, unsharp masking is a very useful technique for obtaining object boundaries.

Once the object is delineated by edges, the centroid or particle position can be measured by region shrinking and skeletonization using morphological image processing, or by geometric analysis. Either approach appears to be able to provide results with comparable accuracy and precision using off-the-shelf image-processing software for filtering, edge detection, and anamorphic processing.

For subsequent evaluation of derivative data such as vorticity, the initial velocity field should be known to an accuracy of typically less than 0.5% because numerical differentiation amplifies errors. To achieve such accuracy, it is necessary to consider all steps in the processing sequence indicated in Figure 2 and to correct for nonlinearities in recording. Unfortunately, almost all published accounts on particle tracking neglect to consider this step, even when computing vorticity data. Since errors in the photographic recording of the particles tend to propagate through the processing sequence and may even get amplified, care should be taken to account for them. Another important source of error in postprocessing of velocity fields is caused by interpolation of the velocity vectors onto a regularly spaced grid. This step is frequently carried out to transform a randomly spaced velocity field onto a grid suitable for computing derivative data. These errors can be reduced by more dense seeding of the flow, as described in the section on speckle velocimetry, or by computing the vorticity field on a randomly spaced grid at only those locations where the velocity has been measured. This approach has not been reported in the literature, but it appears to have merit when accurate vorticity data are desired.

2.3 *Laser Speckle Velocimetry*

In laser speckle velocimetry a particle-laden flow is illuminated by a sheet of laser light, and scattered radiation is recorded on film, or more recently in photorefractive materials for real-time operation (Collicott & Hesselink 1987). The laser is flashed twice to produce a double-exposure image. Many particles are present per resolution cell, which is determined by the geometry of the imaging optics and the wavelength of light. According to Huygens' Principle, particles illuminated by the laser sheet emit secondary waves, which are coherently superimposed on the image plane. Since the phases of all waves arriving at a single point on the film form a random distribution, the resulting intensity has a random spatial distribution too.

This pattern, referred to as a speckle pattern, is well characterized mathematically (Dainty 1975, Goodman 1985). Under the assumption that the particles track the flow, the two images represent the fluid displacement that occurred between exposures. From the displaced speckle pattern, the magnitude of the velocity field is computed. The velocity direction is not readily available unless the two images are shifted between exposures to produce a bias offset (Adrian 1986).

As an alternative to film recording, direct imaging on electronic detectors, referred to as electronic speckle metrology, is feasible in solid-mechanics applications, but application to fluid mechanics is presently limited to rather simple flows. The present resolution of the cameras is limited and prevents accurate measurements to be made in fluids. Alternatively, holographic recording provides three-dimensional information when an extended beam of light illuminates the flow. The advantage of this method is that forward-scattered light is used for imaging instead of the less efficient scattering normal to the laser sheet. In either case, the exposure time for each recording may be so short that the fluid particles are frozen in position, or alternatively it may be long enough to produce particle streaks. From these images velocity is determined in a variety of ways.

In one approach, double-exposed speckle patterns are illuminated with a small laser beam and intensity is measured at the back focal plane of a positive lens. At that location, the spatial Fourier transform of the image irradiance is measured with an electronic camera, such as an array of photodetectors connected to a digitizer and computer system. The image pattern consists of fringes superimposed on a noisy background and a DC bias referred to as "pedestal." The orientation and period of the fringes determine the local velocity vector averaged over the area of illumination of the probe beam; the velocity direction is perpendicular to the local fringe orientation, and its magnitude is inversely proportional to the fringe spacing. By scanning the probe beam in a raster fashion, the complete flow field is surveyed.

Alternatively, Collicott & Hesselink (1986) and Hesselink (1987a) used an anamorphic optical processor involving cylindrical lenses and a sheet of laser light to probe the double-exposure speckle pattern. In this case, the velocity distribution along a line in the flow is measured. The complete velocity field is then obtained by a one-dimensional line scan. This approach is particularly useful when combined with photorefractive recording of the double-exposure speckle pattern. Photorefractives are reusable materials that store phase information through the mechanism of the linear electrooptic effect. The time response is commensurate with pulsed YAG lasers, allowing essentially real-time operation (Collicott & Hesselink 1987).

In a third approach, Meynart (1980) discussed spatial filtering techniques for the problem of speckle velocimetry. Several superimposed speckle patterns are illuminated with an extended probe beam, and a small aperture is placed in the Fourier-transform plane of the readout system, producing a filtered image. Isovelocity contours result, having a magnitude determined by the position of the small aperture with respect to the optical axis of the system. If only two speckle patterns are superimposed, the brightness of the isovelocity contours decreases because they are broad and the signal-to-noise ratio is poor. Digital image processing improves fringe contrast by contrast stretching and low pass filtering. Fringe visibility, however, still remains somewhat poor when dealing with a double-exposure speckle pattern.

2.3.1 APPROACHES TO PROCESSING OF SPECKLE PATTERNS The central problem of laser speckle velocimetry is to detect a periodic signal in a noisy background. Fringe visibility is usually poor, as shown in Figure 5, and image-processing techniques are applied to enhance fringe contrast prior to determining fringe spacing and orientation.

To focus attention to the main issues, a simple mathematical model of speckle fringes is now presented.

Consider two displaced speckle patterns $s(x, y)$ and $s(x+\delta x, y+\delta y)$, where δx and δy denote displacement between exposures in the x- and y-direction, respectively. Upon illumination with a small collimated probe

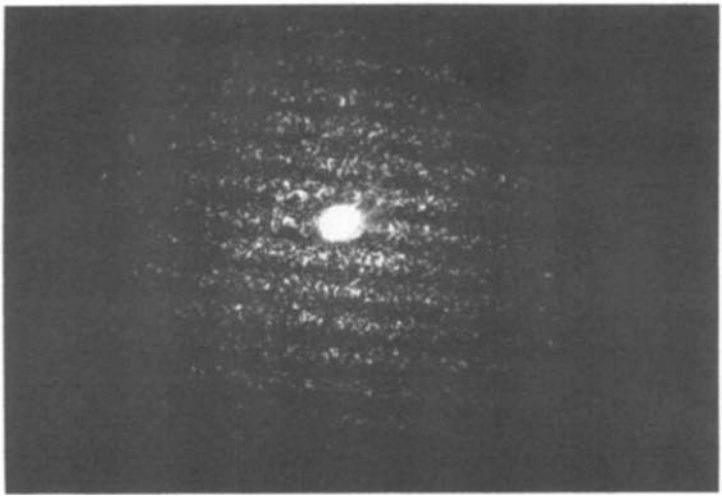

Figure 5 Equidistant fringes obtained from optical analysis of double-exposed speckle pattern.

beam, the intensity pattern in the back focal plane of the positive lens is given by

$$I(\xi,\eta) = A(\xi,\eta) + B(\xi,\eta)\cos^2\left[\frac{\pi}{\lambda f} M(\delta x\xi + \delta y\eta)\right], \quad (1)$$

where M denotes the imaging magnification, λ is the wavelength of the probe light, f is the focal length of the lens, and ξ, η represent the coordinate axes in the back focal plane of the lens corresponding to the x- and y-axes in the object plane, respectively. The bias term $A(\xi,\eta)$ is often referred to as the pedestal and $B(\xi,\eta)$ the diffraction halo modified by the sinusoidal fringe pattern. The fringe pattern carries the pertinent information regarding the fluid motion.

Early on, hybrid processing was used to average along lines parallel to the fringes by using a cylindrical lens. This requires that the fringe pattern is oriented perpendicular to the lens axis. Subsequently, Robinson (1983) devised a simple technique for determining fringe orientation. The image is scanned using a two-dimensional detector array, and it is assumed that the center of the pattern is a maximum. By summing irradiance values along different radial directions passing through the center, the fringe direction is assigned to correspond to the direction associated with the largest sum. Averaging along the fringe increases the signal-to-noise ratio. The spacing is determined from the signal measured perpendicular to the fringe orientation (Kaufmann 1981, Ineichen et al. 1980). This procedure is fast, but accuracy is limited to approximately 1° and the failure rate is somewhat high (about 10%). Substantial improvement over the one-dimensional Fourier technique is achieved by means of a two-dimensional Fourier-transform procedure by which the signal-to-noise ratio is boosted so that reliability is practically 100% and fringe orientation may be measured with accuracies approaching 0.1°. Processing time is considerable, and Huntley (1986) reports an improved method based on the Walsh transform. Results obtained are similar to those of the two-dimensional Fourier-transform technique, but computation time is reduced by almost 70%. The fast Walsh transform does not require multiplications and can be up to an order of magnitude faster than the Fourier transform.

In a complementary image-processing technique, the fringe pattern is digitized on a two-dimensional grid and the spatial phase is detected by comparing signal data with sinusoidally varying reference signals (Toyooka et al. 1985). This technique is an order of magnitude faster than the two-dimensional Fourier-transform technique and provides results with similar accuracy. It was originally developed for communications applications of detecting periodic signals in a noisy background.

An alternative approach for obtaining fringe separation is computing the autocorrelation function of the fringe pattern. This method provides the one-dimensional component of velocity (along the rows or columns), and usually more than two directions are needed to evaluate a two-dimensional velocity pattern because of the relative weak peaks in the autocorrelation signal. For low fringe densities, this approach does not provide good results, and the averaging technique is preferred.

It is important to note here that fringes are straight for the particular readout system employed in the two-dimensional scan method, but that they are curved for the spatial-filtering technique and in the approach of Collicott & Hesselink (1986). In the latter case, the more general fringe-readout approaches described in Section 3 should be considered. Here, we assume that the fringes are straight.

To achieve the goal of accurate velocity measurement, it is almost universally agreed that the pedestal and halo should be removed, if possible, prior to determination of fringe spacing and orientation (Kaufmann 1981). For example, Isacson & Kaufmann (1985) modeled the two-dimensional data-reduction process of fringes superimposed on a diffraction halo. In the noise-free case, for low fringe densities less than six fringes per image and a fringe visibility of less than 0.75, the diffraction halo should be removed in order to keep relative errors in velocity below 1%. In this approach, best accuracy results from using fringe minima for calculation of fringe spacing.

Fringe contrast is also enhanced by recording the fringe patterns nonlinearly on film (Mohanty et al. 1984). An alternative two-step method investigated by Pickering & Halliwell (1984) is useful when few particles are recorded. In the latter method a nonlinear contact print of the fringe pattern can improve fringe visibility considerably.

It is important to note that the diffraction halo multiplies the signal, making the noise term multiplicative as opposed to additive (Isacson & Kaufmann 1985). An effective technique to deal with such noise is cepstrum analysis, in which the logarithm of the intensity field is taken. The advantage of this technique is that when one uses Fourier analysis, the spectrum of the signal is well localized about the origin and the noise term becomes additive. This procedure, however, decreases the signal-to-noise ratio, particularly in the wings of the signal, where the amplitude is small (Meynart 1983). This effect can be reduced by multiplying the logarithm of the signal by a window function, such as the Hamming and Hanning functions. Spectral analysis of the logarithm of the signal allows determination of fluid-flow velocity by spectral analysis, even in cases where the number of fringes is small. In applications involving convection flows, very good results using this method have been obtained by Meynart (1982).

The general properties of fringe formation in speckle photography have been studied by Yamaguchi (1984), and Hinsch et al. (1984) have investigated the use of fringe visibility for obtaining statistical information about the fluid flow. A theorem similar to the Van Cittert–Zernike theorem is devised relating fringe visibility to the viewing direction by the characteristic function of the random displacement field of the scatterers. This technique requires local measurement of fringe visibility for the analysis of such quantities as the degree of homogeneity and isotropy.

An interesting hybrid processing system has been described by Erbeck (1985) in which a rotating ground glass plate reduces speckle noise in the Fourier plane, and in which a density filter with lower transmission in the center than at the edges reduces the envelope of the diffraction halo. The resulting fringe pattern is digitized in binary form, and a correlation technique determines fringe orientation and spacing. Processing time with a small personal computer is approximately two seconds per picture.

2.3.2 ACCURACY CONSIDERATIONS Accuracy of the processing technique is analyzed by considering a periodic signal superimposed on speckle noise. In case there are only a few fringes—that is, no large bias—the standard deviation of the intensity distribution is an estimate of the mean measurement error. This implies, for instance, that when using a readout beam of 0.5 mm the maximum particle displacement is limited to 200 μm. For larger displacements, fringe contrast reduces drastically (Meynart 1983). Fringe visibility is further lowered by differences between the two recorded speckle patterns when using sensitive film with resolution less than that of the optical imaging system.

The noisy background of speckle fringes has been analyzed by Meynart (1985), who includes non-Gaussian statistics in the analysis. However, no new algorithms based on this knowledge have been reported with the objective of improving fringe-readout accuracy. Pickering & Halliwell (1985) have shown that confidence levels of the velocity data can be determined from a modified local fringe visibility curve. This approach is also followed by Arnold et al. (1986) for analysis of nonstationary flows.

As a general conclusion, fringe separation should be measured using fringe minima, since errors are almost four times larger when using fringe maxima.

2.3.3 EVALUATION In speckle velocimetry, the fringes that result from interrogating the double-exposed speckle pattern with a small probe beam are straight and equidistant. On the other hand, those that are produced by the anamorphic optical processor and by spatial filtering are, in general, curved. In either case, the fringes are superimposed on a noisy background, and the pedestal and diffraction halo should be removed from the sampled

and quantized data prior to determining fringe positions. Since the signal-to-noise ratio or fringe contrast is low, all available intensity information should be used for the analysis of the fringe pattern, not just intensity extrema. The Fourier and Walsh transform approaches produce the most accurate results, and they are preferred over fringe-tracking techniques.

The three optical processors discussed here for evaluation of speckle patterns are complementary to each other in terms of ease of operation and the results that can be obtained. The two-dimensional scanning technique using a small probe beam is the most elaborate approach because it requires two-dimensional scanning of the speckle pattern to obtain the full two-dimensional velocity field. On the other hand, the spatial-filtering technique requires no scanning, but only the velocity magnitude can be determined. In addition, more than two (typically four to six) displaced speckle patterns need to be superimposed to get good results. This requires that the flow not change significantly between exposures because otherwise the speckle patterns become uncorrelated and fringe contrast is lost. Alternatively, the anamorphic processor provides the one-dimensional velocity profile directly, and only a one-dimensional scan of the laser sheet is required to map the full field.

2.4 *Laser-Induced Fluorescence*

Laser-induced fluorescence as a spectroscopic tool is effective in combustion research. Numerous studies have been reported in the literature, usually describing point measurements. Field measurements are more difficult to carry out because signal strengths are small, requiring large lasers and sensitive detectors. However, radiometric analysis relating the recorded irradiance to thermodynamic flow or combustion variables is the same for point and field measurements. But so far, digital processing of fluorescence images has been largely restricted to point-by-point data reduction based on spectroscopic approaches, with a few exceptions of field measurements discussed later (Jiménez et al. 1985, Schon 1984).

2.4.1 FIELD MEASUREMENTS Resonance-enhanced fluorescence is capable of providing field measurements using pulsed laser sources and detector arrays or film. Zimmermann & Miles (1980) reported velocity, temperature, and pressure measurements in a sodium-seeded hypersonic helium flow. Quantitative point measurements are obtained by tuning through the sodium D_2 line and fitting the measured profile to a properly

weighted sum of Voigt functions. Signal strength in these experiments is sufficient to allow qualitative flow visualization with a dye laser.

Kychakoff et al. (1982) reported multipoint measurements of species concentration in a plane by using a pulsed dye laser and an image intensifier coupled to a two-dimensional array. Good spatial and temporal resolution are obtained, and quantitative information is computed by processing the recorded signal according to well-known spectroscopic formulas.

Multipoint velocity measurements carried out by using Doppler-shifted laser-induced iodine fluorescence have been reported by McDaniel et al. (1983). A supersonic flow field seeded with iodine is illuminated with a sheet of Ar-ion laser light, and the fluorescent signal is recorded on a two-dimensional photosensitive array. In these experiments, accuracy is limited to about 5 m s^{-1}. This technique requires multiple images to be stored and processed as the laser is tuned in frequency. Signal processing proceeds point by point, and no neighborhood operations are needed to provide velocity at a particular location.

Cheng et al. (1983) performed similar experiments using sodium as the tracer and determined velocity, temperature, and pressure in a supersonic nitrogen jet. This technique also has promise for measuring turbulence characteristics and correlation factors.

Laser-sheet illumination of fluorescing species such as NO and OH also allows measurements of the velocity and temperature fields (Kychakoff et al. 1984).

Extensions of these techniques to other species have been reported by Alden et al. (1984c) for measurement of O_2, followed by H detection (Alden et al. 1984a) and CO (Alden et al. 1984b) in a combusting environment. Atomic hydrogen has been measured by Goldsmith & Anderson (1985) using a two-step saturated fluorescence spectroscopy technique. The image is synthesized by combining one-dimensional linescans recorded sequentially and averaged over time. A similar approach has been reported by Koochesfahani & Dimotakis (1986), using laser-induced fluorescence in a liquid shear flow and a one-dimensional linear photon-detector array. The fluid convects past the detector array and is recorded as a function of time, providing two-dimensional images in a space-time coordinate frame.

2.4.2 EVALUATION Fluorescence techniques can provide accurate species concentration, density, or temperature information, but velocity measurements are at present limited to high-speed flows because the errors in velocity are typically on the order of 5 m s^{-1}. For low-speed-flow applications, particle tracking or speckle velocimetry provides more accurate velocity information. Since the digital image-processing approaches for computing flow density or temperature are similar to those used in one-

dimensional probe techniques, no evaluation is given here, but reference is made to the original sources in the preceding section.

3. LINE-OF-SIGHT REFRACTIVE-INDEX MEASUREMENTS

3.1 *Quantitative Shadowgraphy*

Shadowgraph images record the Laplacian of the index of refraction along the line-of-sight. In the general case, three-dimensional spatially resolved information cannot be extracted from such an image unless multiple views of the object are measured using tomographic reconstruction techniques (see Section 4). However, shadowgraphs of homogeneous and isotropic turbulence can be analyzed using an optical processor to yield correlation functions of the density fluctuations (Uberoi & Kovasznay 1955).

By studying wave propagation through a random medium and solving an inverse problem, we can obtain statistical information regarding a spatially confined random index-of-refraction field from a shadowgraph photograph (Hesselink & White 1983). A laser is used as the light source, and digital image-processing techniques are implemented to reduce the data measured by scanning the photograph with a microdensitometer. In particular, the three-dimensional power spectrum of the medium is computed from the two-dimensional spectrum of the intensity fluctuations on the film.

The result of the analysis is rather simple and easy to implement. The three-dimensional spectrum of the medium is related to the two-dimensional spectrum of the image by dividing each spectral component by the value of the frequency raised to the fourth power and by a scaling factor determined by the geometry of the scattering configuration:

$$S_3 = \frac{6\pi S_1(q)}{[1+3\delta(1+\delta)]D^3 q^4}, \tag{2}$$

where q denotes the spatial frequency, S the spectrum, D the thickness of the medium, $\delta = \hat{D}/(D-1)$, and $\hat{D}$ is the distance from the entrance of the medium to the shadowgraph plane. This result is applicable in the Fresnel zone of the turbulent flow, and it can be used even if a partially developed caustic pattern is formed as a result of random focusing of the wave front. To account for the nonlinear recording characteristics of the photographic medium, the technique is calibrated using the measured Hurter-Driffield curve before carrying out digital processing of the data. Though the correlation function and the spectrum form a Fourier-transform pair, in

general noise consideration prohibits one function being computed from the other.

3.2 *Interferometry*

The information of interest in quantitative analysis of fringe patterns is the phase distribution encoded in the intensity or a derivative of this phase at arbitrary positions in the interferogram.

The irradiance distribution rccorded on film takcs on the form

$$I(x,y) = A(x,y) + B(x,y)\cos[P(x,y)], \tag{3}$$

where $A(x,y)$ describes the slowly varying background illumination, $B(x,y)$ is the envelope related to fringe visibility, and $P(x,y)$ represents the phase function of interest. In general, interferometric fringes are not straight (as shown in Figure 6), necessitating different approaches to digital fringe readout than used for analysis of speckle velocimetry fringes.

3.2.1 APPROACHES TO PROCESSING OF INTERFEROMETRY FRINGES In the generic approach to fringe readout, fringes are skeletonized and labeled using fringe tracking or morphological image processing. The phase function $P(x,y)$ is determined from the skeletonized data by linear-regression techniques. These methods proceed by data preprocessing, usually in the form of digital filtering, to improve fringe quality, followed by either data interpolation to obtain accurate representations of fringe data between cxtrema or morphological processing to skeletonize the pattern into binary

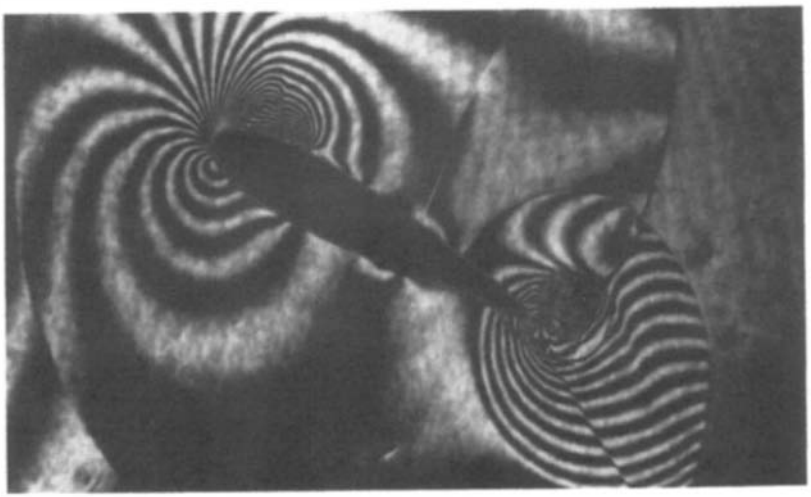

Figure 6 Interferogram of shock-wing interaction. Courtesy of Mandella (1987).

regions for reducing data content. In the latter case, either the maxima or the minima are retained (or both). Finally, fringes are labeled automatically or interactively, and data reduction is performed for measurement purposes.

Major difficulties arise due to noise contamination and slow variation of $A(x, y)$ and $B(x, y)$ over the image. Several approaches are available to deal with these challenges.

The major challenge for automated fringe-readout procedures is the unambiguous measurement of phase; from single interferograms it is usually not possible to uniquely determine whether or not the phase increases or decreases by 2π between consecutive fringes. In other words, the phase is known modulo 2π. A solution to resolve this ambiguity is provided by heterodyne detection, in which a bias phase shift is introduced for unique phase unwrapping from intensity data. In this case the image-processing procedure is much simplified, but at the expense of a more complicated data-acquisition procedure.

Excellent reviews regarding all aspects of interferometry have been given by Vest (1979) and Reid (1986), among others. Numerous optical architectures are used in experimental procedures, coupled with digital image-processing schemes optimized for particular applications. Important approaches are briefly discussed here.

Noise removal is a common preprocessing step, usually involving filtering techniques (Becker et al. 1982) or the superimposition of several shifted patterns (Kreis & Kreitlow 1979, Choudry 1981). In cases where the fringes are nearly straight, one-dimensional approaches suffice (Bernal & Loomis 1977, Augustyn 1979). Extensions to two dimensions have been reported by Jones (1977), Muller & Saackel (1979), and Watanabe et al. (1979).

Grishin et al. (1974) used full two-dimensional data and gray-scale information by computing the cross correlation between an aperture function (usually a rectangle) placed over the data and the pattern itself. Fringe location is then determined by rotating and translating the aperture over the fringes until maximum correlation is achieved.

Interactive approaches have been described by Funnel (1981), and interpolation techniques using Bézier polynomials by Sollid (1975). In the case of dense fringe patterns, such as those obtained with a bias offset in the position of the reference beam of double-exposure holographic interferograms, Fourier-transform techniques are useful (Takeda et al. 1982). Fourier techniques make use of all fringe information, not just extrema, and are therefore the method of choice whenever a sufficient number of fringes is available for processing.

Mertz (1983) suggested a fitting procedure using sinusoids, and Macy

(1983) has described a simple recurrence relationship for phase unwrapping. Morphological approaches, including symmetric pixel-eroding procedures, have been reported by Pavlidis (1977), Arcelli et al. (1975), and Mastin & Ghiglia (1985).

Various approaches to fringe tracking can be found in works by Trolinger (1985), Yatagai & Idesawa (1982), Yatagai et al. (1984), Button et al. (1985), Nakadate et al. (1983), and Cline et al. (1982).

Most fringe-recognition systems encounter difficulties with nonuniform irradiance background distributions and noise. Fringe brightness and visibility may vary across the image because of a variety of effects, including nonuniform object illumination and a nonuniform reference or reconstruction wave in holographic applications. The problems are particularly acute when few fringes are present and optical phase information is desired throughout the interferogram, not just at the peaks and valleys. In flow-visualization applications the number of fringes per unit area is usually low, making these problems particularly pressing for tomographic applications, which require optical phase data throughout the pattern. This often requires data smoothing and interpolation.

A solution to this problem (Schemm & Vest 1983) involves using a one-dimensional nonlinear regression technique on which a function of the form

$$I(x) = B(x) + E(x)\cos[Q(x)] \tag{4}$$

is fitted to the data, where $B(x)$, $E(x)$, and $Q(x)$ are low-order polynomials. Here $B(x)$ describes the variation in background illumination, $E(x)$ is the envelope related to fringe visibility, and $Q(x)$ represents the phase function of interest. Application of nonlinear regression techniques requires careful consideration of noise factors, and good results are frequently only obtained when dealing with a small number of fringes, typically less than five per region over which the technique is applied.

Several of the difficulties associated with phase unwrapping in complicated and noisy patterns may be avoided by using heterodyne interferometry (Dändliker 1980). The intensity of each point in the image is determined for at least three different phase relationships of the reference wave. The measured irradiance is described by

$$I_N(x, y) = I_0(x, y)\{1 + m(x, y)\cos[\phi(x, y) + \phi_N]\}, \tag{5}$$

where ϕ_N denotes the phase shift in the reference wave ($N = 1, 2, 3$), and $\phi(x, y)$ is the desired phase distribution. The phase of the wave in the interferogram, $\phi(x, y)$, is then found at each point (x, y) by computing

$$\phi(x,y) = \arctan^{-1}\left[\frac{\sum_{N=0}^{k} I_N(x,y)\cos(2\pi N/k)}{\sum_{N=0}^{k} I_N(x,y)\sin(2\pi N/k)}\right]. \quad (6)$$

The value of k is chosen to minimize data-acquisition times for a given required resolution and is typically three or higher (Thalmann & Dändliker 1985a,b, Dändliker & Thalmann 1983, 1987, Dändliker et al. 1982, Reid 1986).

A drawback of the heterodyne technique is that several images need to be recorded. In some applications this is not possible. Alternatively, the object and reference beams are arranged to make a substantial angle with respect to each other, and the information of phase is encoded as a deviation in the straightness of the fringes. The FFT technique developed by Takeda et al. (1982) is particularly useful for analysis of these fringes.

3.2.2 EVALUATION At present, heterodyne interferometry provides superior results compared with Fourier transforming or fringe-tracking techniques. It is the method of choice in terms of simplicity in processing, accuracy, and the precision with which the amplitude and phase of the optical wave can be measured. Elaborate fringe-readout and phase-unwrapping techniques are not needed for data reduction, and the phase is measured directly and unambiguously. This superior performance, however, comes at the expense of increased complexity of data acquisition by requiring at least two reference beams or, alternatively, frequency modulation during recording.

In case heterodyne detection is not feasible, an alternative approach based on Fourier or Walsh transforming is recommended. Both techniques provide good results of comparable accuracy, but Walsh transforming is substantially faster than Fourier transforming. In particular, the Fourier transform technique developed by Takeda is powerful and simple to implement. The precision of these methods depends strongly on the number of fringes that are visible in the image, and at least four to six fringes are needed to achieve good results. In applications where the object is weakly refracting, accuracy may be improved by introducing a bias pattern to increase the number of fringes in the interferogram. In holographic interferometry this is best achieved by varying the angle of the reference wave between the two exposures. The bias fringe pattern is then subsequently removed by digital filtering to obtain a zero-offset interferogram from which the phase is extracted.

Fringe-tracking techniques generally provide the least accurate results because only the extrema in the fringe pattern are used for phase deter-

mination. In general, elaborate and semiautomated techniques are required to obtain phase measurements at maxima or minima with similar accuracy as those achievable with transform techniques. The phase at intermediate points must then be obtained by interpolation or by fitting a sinusoidally varying intensity pattern to the skeletonized fringes. In our experience, fringe-tracking approaches have not provided accurate enough results for tomographic applications, where the phase must be known throughout the fringe pattern.

4. TOMOGRAPHY

Tomography allows the distribution of physical parameters such as density, absorption coefficient, or brightness of a three-dimensional object to be determined from line-of-sight measurements. Often a set of line integrals of such distributions can be obtained from appropriate physical measurements. A set corresponding to a particular angular view is called a projection; multiple projections are needed to reconstruct the image.

The first analytic solution for tomographic reconstruction was published by Radon (1917). In 1956, R. N. Bracewell applied tomography to radio astronomy to image microwave emission from the Sun (Bracewell 1956).

Since the early 1960s tomographic image reconstruction has been applied to radiologic imaging (Barrett & Swindell 1981, Rob 1985), geology (Dines & Lytle 1979), oceanography (Munk & Wunsch 1979), and industrial imaging (see the special issue of *Applied Optics*, Volume 24, 1985).

Procedures for image reconstruction include convolution back projection, algebraic reconstruction, and Fourier approaches (Hesselink 1987b, Herman 1979, Macovski 1983). These methods provide exact results when an infinite number of projections are used and the sampling interval approaches zero. In practice, these conditions cannot be met and alternative approaches have been developed. Examples include iterative approaches such as the algebraic reconstruction technique (ART) (Gordon 1974), simultaneous iterative reconstruction technique (SIRT) (Gilbert 1972), iterative optimization codes using the constraint of maximum entropy and a priori knowledge (Frieden & Zoltani 1985), and series-expansion techniques (Lewitt & Bates 1978). Direct methods are faster than iterative approaches but often do not perform as well for limited view-projection data (Oppenheim 1977).

In this review we limit ourselves to optical tomography applied to fluid flow. A more detailed discussion may be found in Hesselink (1987b). Optical tomography uses optical waves for recording of the projections.

In contrast with X rays, the wavelength of visible light is much longer, so that in practical applications diffraction may need to be considered in the reconstruction algorithms. This may substantially complicate data-acquisition systems and data processing.

Optical tomography of fluid flows provides a means for making classical line-of-sight measurements quantitative. Shadowgraph, schlieren, interferometry, and absorption methods may all be used to obtain multiple views of the object. Measurement of the complex part of the index of refraction (absorption) with a tunable laser source allows density, temperature, or concentration measurements to be made in multicomponent flows. Phase measurements or derivatives thereof may be carried out by using nontunable sources.

One of the early applications of image reconstruction from projections was reported by Maldonado & Olsen (1966) and Olsen et al. (1968), who used a series-expansion technique to reconstruct a plasma flow from emitted intensities in an asymmetric argon arc. Rowley (1969) and Wolf (1969) used Fourier transforms to reconstruct transparent phase objects from interferometry data. Wolf's method solves an inverse problem using the Born approximation, and high-resolution inversion techniques have been discussed by Dändliker & Weiss (1970). Shtein (1972) and Vest (1974) discussed early work on image reconstruction from holographic interferometry data. Sweeney & Vest (1973) reconstructed the temperature field in a convective plume above a heated plate submerged in water using holographic interferometry data.

Model studies have been reported by Stuck (1977) and Byer & Shepp (1979) on absorption optical tomography for remote monitoring of air pollution. Snyder & Hesselink (1984) investigated tomographic reconstruction of the flow around a revolving helicopter rotor blade when only an incomplete set of projections is available. This work includes an iterative algorithm to account for ray bending due to the shock. Vest (1975, 1985) and Cha & Vest (1979) also studied the effect of ray bending on the tomographic reconstruction of flow fields. Supersonic and transonic aerodynamic flow fields have been imaged by Collins and coworkers (Matulka & Collins 1971, Jagota & Collins 1972, Kosakoski & Collins 1974). More recently, Kittleson & Yu (1985) reconstructed the flow around a revolving helicopter rotor blade using convolution back projection, and Modares et al. (1985) have done likewise with iterative approaches.

Other fluid-mechanical applications include the work of Alwang et al. (1970) on slot flames, by Zien et al. (1975) on supersonic flow over a cone, and by Emmerman et al. (1980), Santoro et al. (1981), Semerjian et al. (1981), and Ray & Semerjian (1983) on temperature and concentration methods in a combusting environment using absorption tomography. In

this last study, a limited number of views provide time-averaged images of physical parameters. Bennett & Byer (1984, 1986) and Bennett et al. (1984) studied fundamental noise aspects of fan-beam tomography as applied to concentration measurements in iodine-seeded flows. Beam-deflection techniques allowed Faris & Byer (1986) to study flames. Hertz (1985) measured temperature in a flame using interferometry and an asymmetric electric-field distribution in dielectric liquids using the Kerr effect (Hertz 1986).

Other applications include aerosol measurements by Willms (1981), interferometric density in a Rayleigh-Bénard convection cell by Kirchartz et al. (1981), and measurements in a boundary layer by Cha & Vest (1981). Infrared emission from a flame was used by Uchiyama et al. (1985) to measure temperature.

Tomographic measurements so far have only been applied to time-averaged or stationary flow fields. Time resolution is limited because data-acquisition schemes either require long data-averaging times or else only a few projections are obtained in a short time span and thus the experiment must be repeated to measure all necessary views. Snyder & Hesselink (1985) discussed an optical-data acquisition scheme to overcome these limitations, and this system is capable of making time-resolved tomographic measurements in turbulent flows using 36 viewing angles obtained in less than 300 μs with a 1-W argon laser (Snyder & Hesselink 1987).

Optical tomography requires in-plane optical beams to probe the flow. In this respect it differs from scattering techniques using laser-sheet illumination, in which the recorded image is obtained by collecting scattered radiation outside the plane of illumination. In certain applications, such as the measurement of hot exhaust plumes of jet engines, in combustion experiments, and in tokomaks, tomography may provide a means for measuring flow quantities that cannot be obtained conveniently with scattering techniques.

4.1 *Principles of the Method*

For this discussion of the method, assume the recording geometry shown in Figure 7. The distribution of the physical property in the medium is described by $g(x, y)$, which for the moment we assume to be a two-dimensional function; extension to three dimensions by stacking planes is discussed later.

The results of measurements are estimates of line integrals along lines of known location, often referred to as projections. The line along which $g(x,y)$ is measured is denoted by u and can be expressed in terms of R, the distance from the origin, and the angle θ. We can compute the optical pathlength along u as follows:

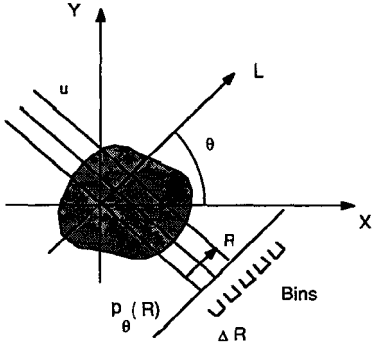

Figure 7 Tomographic recording configuration.

$$p_\theta(R) = p(R,\theta) = \int_{-\infty}^{\infty} g(R\cos\theta - u\sin\theta, R\sin\theta + u\cos\theta)\, du$$

$$= \int_{-\infty}^{\infty}\int g(x,y)\delta(x\cos\theta + y\sin\theta - R)\, dx\, dy. \qquad (7)$$

The object of tomography is to recover $g(x, y)$ from projection data $p_\theta(R)$.

The simplest case of axially symmetric data was solved by Abel in 1826 (Vest 1974). Radon (1917) provided an analytical result in the general case and showed that the object can be recovered from the projections, provided an infinite number of projections are known with arbitrary accuracy. In practice, of course, this is never possible, and approximate reconstruction methods are needed. Under these conditions no unique solution exists, and for a given data set several objects can be reconstructed, all consistent with the data. The differences from the ideal or desired image manifest themselves as artifacts. The specific form of these artifacts depends on the particular reconstruction algorithm used.

Several reconstruction schemes have been devised; the most popular ones are the algebraic reconstruction technique (ART), filtered and convolution back projection, FFT techniques, maximum entropy, and other iterative approaches.

Here, the essence of the technique is illustrated using the Fourier-transform technique. However, modifications such as convolution back projection have enjoyed widespread popularity for their speed and accurate reconstructions, particularly in medical applications. In fluid-mechanics applications several algorithms may have to be combined to deal with noisy and incomplete data and to account for diffraction and ray bending (Snyder & Hesselink 1984).

In an idealized case the projection $p_\theta(R)$ is determined by

$$p_\theta(R) = \iint g(x,y)\delta(x\cos\theta + y\sin\theta - R)\,dx\,dy$$

$$= \int_0^{2\pi}\int_0^{\infty} g(r,\phi)\delta(r\cos(\theta-\phi)-R)r\,dr\,d\phi, \tag{8}$$

where $p_\theta(R)$ represents projection information in the θ direction. In this calculation, integration is performed along $x\cos\theta + y\sin\theta = R$. In polar coordinates, the delta function $\delta(r\cos(\theta-\phi)-R)$ selects the desired line to produce a line integral.

The Fourier-analysis approach to image reconstruction is based on a basic property of transform pairs, which is explained by considering $g(x,y)$ and letting $G(fx,fy) = F\{g(x,y)\}$. Then

$$G(fx,fy) = \iint g(x,y)e^{-i2\pi(f_x x + f_y y)}\,dx\,dy,$$

or in polar coordinates

$$G(fx,fy) = G(\rho,\beta), \qquad f_x = \rho\cos\beta, \qquad f_y = \rho\sin\beta,$$

$$G(\rho,\beta) = \iint g(x,y)e^{-i2\pi\rho(x\cos\beta + y\sin\beta)}\,dx\,dy \tag{9}$$

$$= \iiint g(x,y)\delta(x\cos\beta + y\sin\beta - R)e^{-i2\pi\rho R}\,dx\,dy\,dR.$$

Now compare (8) and (9) to get

$$G(\rho,\beta) = \int p_\beta(R)e^{-i2\pi\rho R}\,dR,$$

$$G(\rho,\beta) = F_1\{p_\beta(R)\}, \tag{10}$$

where F_1 denotes the one-dimensional Fourier transform. Then the Fourier transform of a projection at angle β forms a line in the Fourier plane at exactly the same angle β (Figure 8). From this observation we now deduce the procedure for tomographic reconstruction:

1. Measure projections such that the corresponding Fourier-transform plane is filled.
2. Back transform the result using a two-dimensional FFT to get $g(x,y)$, i.e.

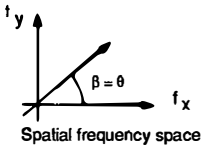

Figure 8 Coordinate transformation.

$$g(x,y) = \iint G(fx,fy)e^{i2\pi(f_x x + f_y y)}\, df_x\, df_y$$

$$= \int_0^{2\pi} d\theta \int_0^{\infty} G(\rho,\theta)e^{i2\pi\rho(x\cos\theta + y\sin\theta)}\rho\, d\rho. \tag{11}$$

The difficulties with this approach are the need for several coordinate transforms and the computational effort required for good reconstruction. Consequently, approximate methods are used such as convolution back projection, which is both a fast technique and provides good results. It is one of the most popular image-reconstruction methods for both medical and flow-visualization applications.

A detailed derivation is beyond the scope of this review (Hesselink 1987b, Macovski 1983), but the results are worth noting:

$$g(x,y) = \int_0^{\pi} d\theta \int_{-\infty}^{\infty} \left[\int_{-\infty}^{\infty} F_1\{p_\theta(R)\}\,|\rho| e^{i\,\pi\rho R} \right] \times \delta(x\cos\theta + y\sin\theta - R)\, dR$$

and

$$g(x,y) = \int_0^{\pi} d\theta \int_{-\infty}^{\infty} F_1^{-1}[F_1\{p_\theta(R)|\rho|\}]\delta(x\cos\theta + y\sin\theta - R)\, dR. \tag{12}$$

The image is reconstructed by first computing the one-dimensional Fourier transform of each projection and multiplying it by $|\rho|$. Then the inverse transform of the result is computed, followed by a back-projection operation. Since (12) can be rewritten by observing that

$$F_1^{-1}[F_1\{p_\theta(R)\}\,|\rho|] = p_\theta(R) * F_1^{-1}\{|\rho|\}, \tag{13}$$

convolution operations may be used for the reconstruction.

Unfortunately, the inverse transform of $|\rho|$ does not exist, and thus approximations to this function (Macovski 1983) must be made for image reconstruction.

Artifacts are introduced when only a limited number of projections are available. The particulars of these artifacts depend on the reconstruction

algorithm. For convolution back projection, missing projections introduce radial stripes in the reconstructed image. These stripes have their origin in the one-to-one correspondence between lines in Fourier space and the projections. An example illustrating the effect of the number of projections on the quality of the reconstruction is shown in Figure 9. The tomographic process is simulated by computing the reconstructed image of a test case shown at the far right of the second row in Figure 9. The results show a varying degree of fidelity depending on the number of projections and the noise level.

In medicine, where X rays are used at a wavelength short compared with the dimensions of physical objects, the photon paths are essentially straight lines. For fluid-mechanics applications using optical probe beams, rays may not be straight, requiring that reconstruction codes be modified. Ray bending becomes significant when the deviation of a ray from a straight line is larger than 1 bin at the location of the projection measurement. (The projection is sampled at intervals ΔR referred to as bins, shown in Figure 7.) In this case, conventional reconstruction algorithms for X-ray tomography will try to back project the data along a straight line,

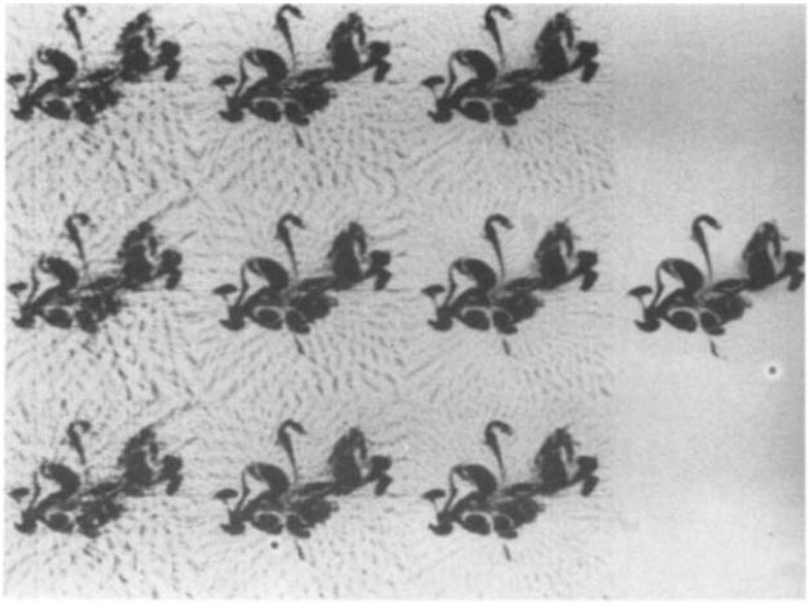

Figure 9 Effect of number of projectives on quality of the reconstructed image. The three rows show reconstructions for noise levels of 5, 2, and 5% (with median filtering), respectively; the columns represent reconstructions with 20, 30, and 40 viewing angles. The radial artifacts are caused by the convolution back-projection technique. The original test object is on the right of the image.

which renders the projection data inconsistent with the physical object. Under these conditions severe artifacts may occur.

This problem has been extensively studied by Vest (1979), who considered the effect of ray bending on interferometry and tomographic reconstruction of strongly refracting objects. A particularly difficult problem to deal with is ray crossing, or caustics. These difficulties may be alleviated by using an imaging configuration.

For instance, ray bending due to shock refraction can be compensated for by imaging or using an iterative algorithm to correct for nonrectilinear wave propagation (Snyder & Hesselink 1985). The method of back propagation discussed by Devaney (1983) is also particularly effective in reducing refraction effects.

4.2 *Evaluation*

The quality of tomographic reconstructions is largely dependent on the reconstruction algorithm, the number of views used, the noise level and resolution of the projections, and the flow topology. Generally speaking, image quality improves with increasing number and quality of the projections. In particular, for reconstruction of flows with fine detail and sharp discontinuities, a large number of projections may be needed. For example, sharp discontinuities such as shocks and thin interfaces between two different fluids tend to cause streaky patterns in the reconstructed flow. These artifacts may be estimated by carrying out a modeling study in which the quality of the reconstruction is studied as a function of the number of views and resolution as well as the noise level of each projection. The artifacts caused by the reconstruction may be further reduced by post-reconstruction image processing such as median filtering and image enhancement, often without significant loss in detail or fidelity.

A peculiarity of currently developed reconstruction schemes is that all projections must lie in a plane, usually along an arc of 180°. This need for optical access implies that walls containing the flow must be optically transparent and should not distort the probe beam. Thus optical windows should be made thin to reduce ray bending. Because of this requirement, measurements of flows in round ducts are difficult to achieve unless optical elements are introduced into the probe beam to correct for ray refraction caused by the curved walls. It is, however, not necessary to probe the flow with collimated light, and fan-beam tomography can provide excellent results as well. The trade-off is usually one of determining the optimum geometry of the optical apparatus under a set of space constraints.

In most flow applications, holographic interferometry has been used as the probing technique for measuring temperature, density, and concentration. Although interferometry is a well-developed diagnostic tool

and is widely used for qualitative flow visualization, data reduction is often a complicated and time-consuming task, in particular for turbulent flows with considerable structure. Therefore other approaches, such as absorption and deflection tomography, should be considered viable alternatives because they require much simpler data-reduction schemes. For example, absorption tomography is very well suited for combustion research because by tuning a laser to a particular absorption line of an intermediate species or reactant, species-specific measurements of concentration or temperature may be made, and data reduction is not nearly as complicated and time consuming as for holographic interferometry. Emission tomography is also an attractive method for combustion research because no external probe beam is required to obtain the projections.

From the projections the flow may be reconstructed in a variety of ways. The most widely used reconstruction algorithm is convolution back projection. It is a fast and easy-to-implement approach, which in this author's opinion should be tried first; for the flow around a revolving helicopter rotor blade and a coflowing jet, we have evaluated the quality of reconstruction when using various reconstruction schemes and have found no significant improvement for one approach over another. In those applications where the projections are not uniformly spaced about the object or where projections are missing, convolution back projection can still provide good results, provided the missing projections are generated (for example, by interpolation of available data). Alternatively, the ART or the maximum entropy method tend to produce good results for these reconstructions but at the expense of considerably more computation time. In our experience we have always achieved comparable results with direct and iterative approaches when using postreconstruction image-enhancement techniques, such as median filtering to remove isolated noise spikes.

In addition to complications arising from incomplete data, difficulties also occur when the rays are bent. All reconstruction algorithms considered here are based on the assumption that the rays are straight. In combusting and two-phase flows or in flows with large density gradients, this may not be true as a result of refraction. In these cases, the reconstruction algorithms need to be modified. As an example of an approach in which the effects of ray bending are reduced, the image is first reconstructed under the assumption that the rays are straight. Then the rays are traced through the medium and the projections are computed including the effects of ray bending. The measured projections are subsequently compared with the computed ones and are updated to account for the differences. The updated projections are then used to compute a new reconstruction. This process is repeated until the difference between two sequential reconstructions is below a threshold value. Using this approach, much improved results have

been obtained for reconstruction of the flow around a revolving helicopter rotor blade. In this application, rays nearly parallel to the shock are bent rather strongly because the gradients in the density (and, therefore, the index of refraction) are perpendicular to the ray paths. Unfortunately, in general one cannot be assured of convergence of this approach, and each application needs to be investigated to determine the effects of ray bending. Alternatively, the effects of ray bending may be reduced substantially by using a lens that images the object onto the measurement plane for each projection. This approach should always be tried first if an imaging configuration can be implemented.

Difficulties also arise when the probe beam does not cover the full flow-field cross section. In this case severe artifacts often contaminate the reconstruction. In addition, evaluation of interferograms becomes very difficult because reference information about density or temperature in the unperturbed region is missing. Since tomography reconstructs the full flow field, a smaller interior region cannot be reconstructed by only probing that section of the flow. However, from a coarse representation of the complete flow, a smaller subsection may be reconstructed with higher resolution (using additional data) by a technique referred to as "onion peeling."

5. DIGITAL IMAGE PROCESSING

Three-dimensional flow fields are difficult to conceptualize and comprehend. In all but the simplest flows, velocity or streamline patterns are too complicated to be understood from direct graphical presentation in the form of particle traces or two-dimensional cross sections of the velocity field. The need for understanding of such multidimensional data sets has become more acute with recent advances in high-speed optical data-acquisition systems and with the increasing power and speed of supercomputers used in the solution of the three-dimensional Navier-Stokes equations. The complexity and large volume of the data generated by these tools require that new techniques be developed to facilitate further study, display, and comparison of fluid-flow data sets.

Numerical data are similar to those produced by modern optical diagnostics, and some of the same flow-visualization techniques have been applied to numerically generated data sets. As an example, paths of particles released in the flow are computed and visualized on graphics terminals in much the same way as hydrogen bubble-flow visualization is used in experiments. A difficulty with this approach is that for complicated flows the particle paths tend to become intertwined and difficult to discern.

In principle, visualization methods equivalent to schlieren, shadowgraphy, and interferometry can be applied to analysis and display of

computational data as well. The flow-visualization images are then computed using ray-tracing techniques. As an example, Snyder & Hesselink (1984) computed the equivalent of optical interferograms for the flow around a revolving helicopter rotor blade and used this information to simulate tomographic experiments. Numerical simulation of flow-visualization techniques has the added benefit that results can readily be used for comparison between experiment and numerical analysis.

For the purpose of discussing the various techniques, we assume that data are available in quantized and sampled form on an ordered sequence of planes. The source of the information may be either experiments or numerical analysis. Furthermore, it is assumed that the scalars at each pixel represent quantized values of a physical parameter of interest, such as pressure, temperature, or density.

A general approach to digital image processing is shown in Figure 1. Since this is a generic outline, most steps are customarily followed during processing, but it is understood that the specific order and steps may vary from application to application.

5.1 *Techniques*

5.1.1 DATA COMPACTION Data compaction is almost always desirable to improve processing speed and reduce memory requirements and may take on a variety of forms.

The simplest, but not always the best, technique is binarization, in which a gray-level image is reduced to two levels (black and white) by either thresholding or edge detection. The choice of threshold level is an important consideration, particularly in images contaminated with noise. Threshold values can be set globally or locally using averages over a number of pixels or based on image statistics. A very powerful and useful technique is selecting the threshold value on the basis of the histogram of gray levels in the image. For instance, in a picture consisting of a dark object on a bright background, the histogram will be bimodal and the optimal threshold lies between the two peaks. In this case, thresholding produces data compaction as well as a means for image classification.

Other approaches are based on decompositions in terms of eigenimages including the Karhoenen-Loeve, Walsh, Haar, Hadamard, Fourier, and Slant transforms and singular-value decomposition. Data compaction is achieved by retaining only the eigenimages corresponding to the largest eigenvalues. Alternatively, image-coding techniques provide a means to achieve data compaction and still retain good image quality.

5.1.2 ENHANCEMENT TECHNIQUES Image-enhancement methods are of an ad hoc nature. Many schemes are available, including contrast stretch-

ing, histogram modification, noise cleaning, filtering, edge crispening, median filtering, false-color representations, and image restoration. These techniques are generally applicable but achieving success is more an art than a science, with trial and error one of the few reliable methods to improve image quality. Noise removal is particularly useful when edge detection is desired. Thresholding techniques do not work well in the presence of strong noise components, and low pass filtering blurs edges. Averaging along edges increases the signal-to-noise ratio without sacrificing image quality and is particularly useful for analysis of noisy fringe patterns.

5.1.3 SEGMENTATION Image segmentation proceeds by grouping pixels having similar properties, such as pixel value, texture, or statistics. Several automated techniques have been developed for this purpose, including region growing, edge, shape, texture, and gradient-based segmentation. Although these methods have been successful in the analysis of natural scenes, they are less useful in fluid-mechanics applications. Flow-visualization pictures do not usually show the same diversity in textural content as natural scenes, and edges are often blurred, making gradient methods difficult to apply. In such cases, critical-point analysis may be more useful for classification.

5.1.4 CLASSIFICATION Once the regions have been identified, they need to be classified. For classification of natural scenes, various approaches have been found useful, including code-book analysis, geometrical reasoning, spectral analysis, and matched filtering. These approaches should ultimately lead to a description of the image. In scene analysis this may be identification of roads, cars, planes, etc. In fluid flows we would like to find large-scale eddies, critical points, and vortices.

5.1.5 IMAGE DECOMPOSITION Image decomposition is a proven technique for pattern recognition and image understanding in two-dimensional applications (Young & Fu 1986). For example, an aerial photograph can be broken up into regions of similar properties that are then classified according to local characteristics, such as surface texture, brightness, and geometry. These characterizations then provide a basis for identifying each region as belonging to a particular class of object, such as "road" or "parking lot," and thus help generate an abstract representation of the scene as a set of these objects and their relationships (Perkins et al. 1986, Herman & Kanade 1986). In fluid-mechanics research, it would be desirable to carry out a similar type of analysis on the vector fields that are central to the understanding of fluid flows. As in scene analysis, one is presented with a large volume of data containing structures to be located,

identified, and characterized, and one would like to have methods of automating the time-consuming process of manually analyzing and describing the data. Both cases also require the application of a priori knowledge about the data being studied to the interpretation process, e.g. that cars are usually on roads or that the vector field is derived from the Navier-Stokes equations (Hesselink & Helman 1987).

5.1.6 THREE-DIMENSIONAL GRAPHICS Flow visualization relies heavily on graphics. Interpretation of processed two-dimensional imagery is usually carried out using graphics techniques such as contour maps, shading, and false-color representations. Since display devices are usually two-dimensional, special approaches are required for representation of three-dimensional imagery. For this purpose the following techniques are well-suited.

Perspective projection is a means of mapping a three-dimensional scene onto a two-dimensional display screen such that distant objects appear smaller than close ones of the same size. This is similar to image formation in optical systems.

Intensity or *color depth-encoding* makes the intensity or color of objects a function of their distance from the view point. Usually, distant objects are made to appear darker than close objects when intensity depth-encoding is used.

Stereopsis is a technique that displays two slightly different images to each of the observer's eyes. The image pair is generated using two view points differing by a few degrees of angular separation. When the image pair is presented to an observer—usually with the aid of an optical device—the observer's brain fuses the pair into a single three-dimensional scene. This technique is powerful, yet easy to implement.

Motion is produced by rapidly displaying a sequence of images from slightly varying view positions. Rotations are particularly helpful for revealing depth relationships.

Hidden-surface removal and *surface shading* model the interaction of light with physical objects. Hidden-surface removal models the opaqueness of most objects familiar to us. Shading models the reflection of light from surfaces.

These techniques may be combined to provide very powerful depth cues.

Holography provides true three-dimensional depth cues and has the potential to be very useful for display of flow-visualization imagery. A hologram may be obtained by direct optical recording or by computing views of a synthetic object that are later combined in a holographic display. Intensity depth-coding and surface shading are effective means to enhance computed holographic displays, too.

5.2 *Two-Dimensional Image-Processing Applications*

Digital image-processing techniques are powerful methods for enhancement and quantitative data extraction of flow-visualization photographs. In the preceding sections, several two-dimensional techniques were discussed; here we briefly consider a few cases that fall outside the scope of the discussion presented earlier. For example, smoke-visualization photographs may be enhanced to determine turbulent large-scale structures in boundary-layer flows using homomorphic image processing (Corke 1981, 1983). Similarly, the density of particles delineating flow structures may be found by applying edge-finding and pattern-recognition techniques (Toulouse et al. 1985, Schon 1986). In case the particles are large enough to be imaged individually, geometrical information may be extracted after classification has been completed. Features such as shape factors, sizes, and position of particles with respect to flow features are of interest (Gennero & Mathe 1985). Other examples include determination of the time history of drop size and the volume distribution of droplets in a spray (Shimizu et al. 1985, Hernan et al. 1985, Biscos et al. 1986). The approaches taken in these studies are useful for three-dimensional image processing as well, and a more detailed account follows in the next section.

One aspect of two-dimensional image processing is to provide humans with a graphic display of information because the human visual system is well adapted to extract structural information from imagery. In many cases, visual display of data is easier to assimilate than a string of numbers, and this suggests that point measurements are composed as an image. Image synthesis is a new approach for interpretation and evaluation of survey data such as pressure, temperature, and velocity obtained at various points throughout the flow. For example, an image may be composed from survey data obtained at various points throughout the flow, making it possible to comprehend complicated flows that otherwise would be much more difficult to discern (Winkelmann & Tsao 1985, Sakata et al. 1985, Crowder & Beck 1985).

A useful attribute for interpretation of flow imagery is color coding. A color is assigned to each pixel on the basis of its value using any of a variety of color-coding schemes (Smith et al. 1985). Since the human visual system is particularly well suited to discriminate between hues, color displays are often more effective in accentuating small pixel amplitude differences than gray-scale displays.

5.3 *Three-Dimensional Image Processing*

Tomography and laser-sheet illumination techniques provide two-dimensional flow cross sections. By sweeping the laser sheet rapidly through the

fluid or by recording a time sequence of images using a stationary sheet and applying a Galilean transformation, a three-dimensional representation of the flow is obtained. Hesselink et al. (1985) reconstructed a coflowing jet from a stack of 40 cross sections using a source-attenuation method. The three-dimensional image was displayed using stereo computer graphics and motion parallax, and the first multiplex hologram of a fluid flow was constructed. Subsequently this approach was followed by Hasen & Graham (1985) for visualization of numerically generated flows.

Agui & Hesselink (1987) have studied the three-dimensional structures in a coflowing air jet. A circular jet of slightly higher velocity than the surrounding coflowing stream is seeded with kerosene smoke and a stationary laser sheet illuminates a cross section of the flow. In this geometry a cylindrical sheet of vorticity is formed at the interface between the two fluids. This sheet is unstable and tends to roll up into vortices that are convected past the stationary sheet. The instability is made periodic by acoustic excitation of the jet.

Scattered radiation from the jet inner fluid is recorded on high-speed motion-picture film; the sequence of images represents consecutive cross sections of the vortical structure. A complete cycle is recorded on 40 images, which are digitized for further processing. The time between exposures is short enough to accurately describe the flow. A Galilean transformation is applied using the convection velocity of the fluid to transform time into a space coordinate. Alternatively, fast sweeping of the laser sheet avoids the need to invoke this transformation (Prenel et al. 1986, Schon 1986).

Once the images are available in numerical form in the computer, the first task is to classify regions in the flow according to the presence or absence of smoke. Smoke is used as a tag for identification of the inner fluid. Pixels are classified as being either "smoke" (white) or "nonsmoke" (black). This step is simple data compression, since the classified data are binary.

Performing this type of classification is a challenge when optimum detail is desired without amplifying noise. As a result of the high diffusivity of smoke in airflows, the fine detail of the inner flow structure is embedded in a low-contrast region of relatively high average luminosity. Classification in this case is carried out using unsharp masking followed by a thresholding operation, and it provides very good results in reasonable computing time.

Digital image processing of the cross sections entails three steps. In the first, background noise is removed by intensity thresholding, which preserves pixel values above a set threshold while nulling all pixel values below it. The second step involves feature enhancement by subtracting the

average local base value in the neighborhood of the pixel under consideration and a subsequent contrast stretch to span the pixel values over the full dynamic range of 8 bits, or 256 gray levels. In the final step a thresholding operation is applied to the enhanced data to perform region classification. Any noise still present tends to be isolated spikes that are removed by nonlinear median filtering.

In this process careful consideration should be given to selection of the threshold value; variations of the threshold value on the order of 30% (producing segmented images that are clearly far from the expected result) may result in variations in the flow quantities of interest, such as the surface-to-volume ratio, of up to 20%.

The determination of the boundary between the two fluid regions is important, since that boundary represents the interface where molecular mixing takes place. In reacting flows the reaction rate is, among other factors, proportional to the interface area between the reactants, and it is easily determined from the segmented images.

The process is visualized in Figures 10 and 11, using a typical cross section. Figure 10 represents both the original digitized image and its classified version, while Figure 11 shows the boundary between the two fluids. The main difficulty that still persists is that very strained portions of the inner jet fail to scatter enough light to be classified as smoke material. Consequently, parts of the jet may appear to be unconnected even though the original image shows a faint smoke bridge between regions. To improve results, morphological image-processing and pattern-recognition procedures might be able to recreate those lost connections, but they would always be obtained at the risk of creating artifacts in the restored image.

5.3.1 SOLID RECONSTRUCTION AND DISPLAY TECHNIQUES Frequently, the first objective of modeling and/or display processes is to produce two-dimensional projections of a three-dimensional model of the described object. The final goal is usually to display the spatial structure in three dimensions, allowing full comprehension of topological features from display of perspective projections.

Reconstruction of a solid out of a series of cross sections can be done in several different ways. An emission-absorption procedure, as described by Hesselink et al. (1985), stacks all the cross sections, one after the other, in an imaginary three-dimensional space. Each slice is previously thickened by the proper amount as computed from the filming rate and the convection velocity. Then, each "voxel" (pixel in three-dimensions, or the minimum addressable volume unit) behaves as a light emitter proportional to the amount of smoke originally present at that location (i.e. light scattered and recorded on the film) and as an attenuator for the light

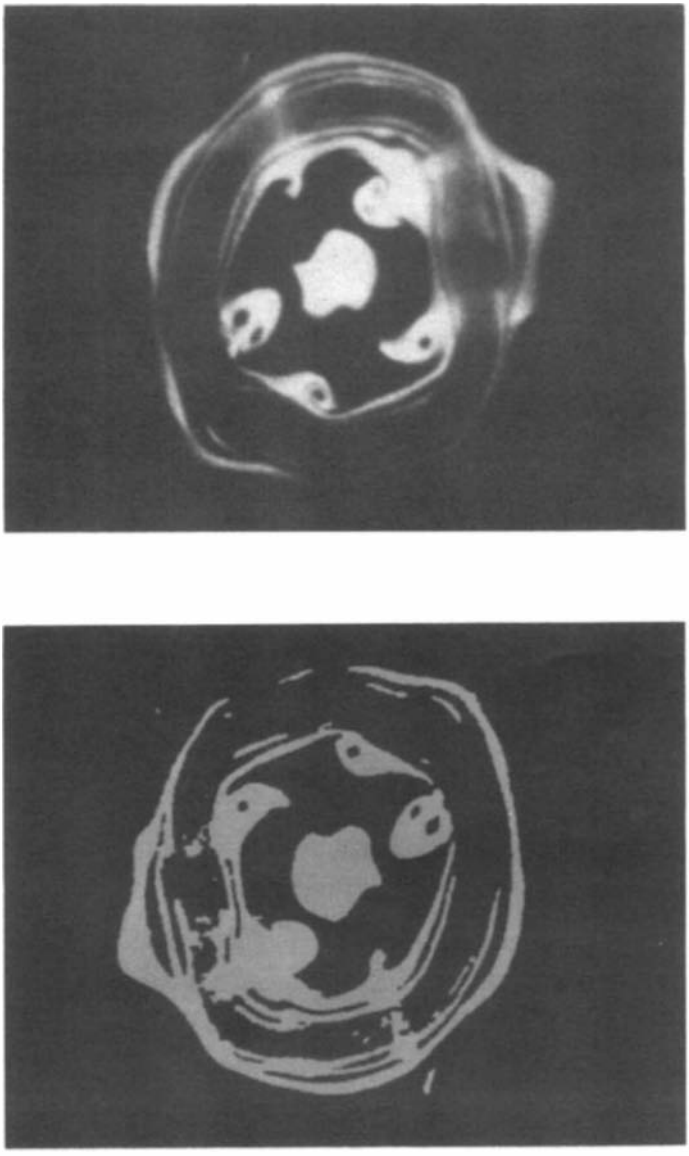

Figure 10 Original (*top*) and classified (*bottom*) version of a selected cross section of the coflowing jet of Agui & Hesselink (1987).

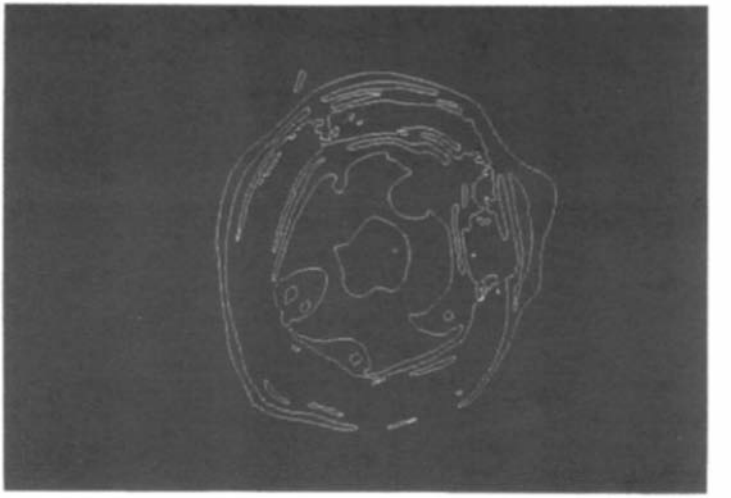

Figure 11 Boundary between inner and outer fluid.

emitted by pixels farther away from the viewer. The result is a view of a solid with an adjustable degree of transparency, which allows information hidden by the external surface of the structure to be seen. On the other hand, it lacks important depth cues produced by effects such as shadows and intensity coding. The source-attenuation method is more suitable for high-contrast images, such as those produced by liquid fluorescence experiments, because if used with low-contrast images, or images with very fine detail, the results are somewhat fuzzy.

Another technique involves analyzing each cross section and reducing it to a set of closed singly or multiply connected polygons whose description is simply an ordered list of points in a plane. In this manner, it is possible to undertake the analysis of the topological evolution from one cross section to the next. This is in the general case an extremely difficult and costly task. If done, a smooth approximation to the real surface of the body is obtained, and it can be represented by three-dimensional rendering techniques (Jiménez et al. 1985, Fusch et al. 1977, Wu & Hesselink 1987, Yip et al. 1986).

For example, Jiménez et al. (1985) reconstructed a three-dimensional representation of the plane mixing layer from a sequence of motion pictures using laser fluorescence. The data base consists of two-hundred consecutive transverse cross sections representing a section of a three-dimensional solid where time is plotted along the third dimension. Time is converted into space using a fixed convection velocity.

Data processing involves radiometric calibration to correct for absorption between the light sheet and the observer, filtering to reduce noise, and classification of regions according to irradiance levels. Thresholding is based on computing the local irradiance gradient (Keffer et al. 1985), and data compaction is achieved by expressing the boundaries between regions in terms of polygons.

A three-dimensional representation of the mixing layer is obtained by stacking the polygonal contours of each cross section. Various forms of three-dimensional representations are known, and they are described by Foley & Van Dam (1982). From each cross section a short prism based on the polygonal cross section is constructed, with a depth equal to the separation between slices. The prisms are then stacked to form a polyhedral body. Hidden-surface removal is used to display the results, and additional depth cues are generated by shading the object using point-source illumination, but no shadows are computed. The resulting unnatural effects of the representation are controlled by judicious choice of the source location with respect to the observer.

In another approach, Yip et al. (1986) used a sequence of slices resulting from Rayleigh scattering to reconstruct gas concentration in a perturbed laminar flame. The flow is reproducible, and a laser sheet is scanned through the flow during repeated experiments to obtain a three-dimensional representation. Rayleigh-scattered light is recorded on a sensitive two-dimensional photon detector, and the recorded digital data are displayed using computer graphics, which involves hidden-surface removal and shading.

The approach of Agui & Hesselink (1987) is somewhere between the two described above. The data (cross sections) are not analyzed in geometrical terms, and each section is processed separately, eliminating the need for finding topological connections. This avoids any danger of information loss and produces some savings in computer time. The process consists of creating a cylinder whose cross section corresponds to the data and whose height is the spacing between slices. The three surfaces of this cylinder (upstream and downstream planes plus the side surface) are then drawn using a z-buffer algorithm for hidden-surface removal (Newman & Sproull 1979). A very convincing representation of the solid is achieved by properly stacking these cylinders, which may be enhanced using a flexible projection algorithm and a lighting scheme that improves the three-dimensional cues. The drawbacks of this approach are that the evolution of the volume between the slices is not described and a sometimes distracting "staircase-look" results. On the other hand, a small amount of discontinuity between adjacent cylinders tends to enhance the stereo cues and improve depth perception, as shown in Figure 12. A smooth rendition of these data can

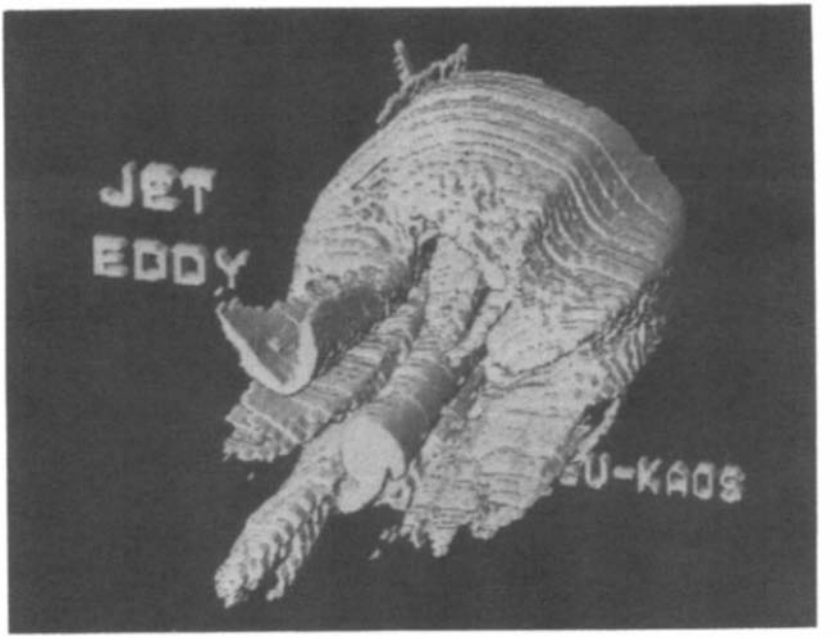

Figure 12 Three-dimensional representation of coflowing jet eddy.

also be made with the technique discussed in Section 5.3.4. From the processed data, cross-sectional planes at any orientation may be computed to reveal the interior detail shown in Figure 13.

Once the representation is available, it provides a powerful aid for the development and analysis of the three-dimensional data set. For instance, Agui & Hesselink (1987) report a numerical analysis based on the vortex-element method to model the instability process of the ring vortex and to provide guidance in the interpretation and understanding of the motion of the longitudinal vortices. In addition, quantitative information, such as the surface-to-volume ratio of the interface between the inner and outer fluid, can be computed.

5.3.2 DEPTH CUEING THREE-DIMENSIONAL DISPLAY TECHNIQUES Substantial improvement in the rendering of the three-dimensional images can be achieved using depth cueing. Depth-cueing techniques used in computer graphics are well-documented (Newman & Sproull 1979, Foley & Van Dam 1982). They include—but are not limited to—perspective projection, intensity or color depth-encoding, stereopsis, motion dynamics, hidden-line or hidden-surface removal, and surface shading. These

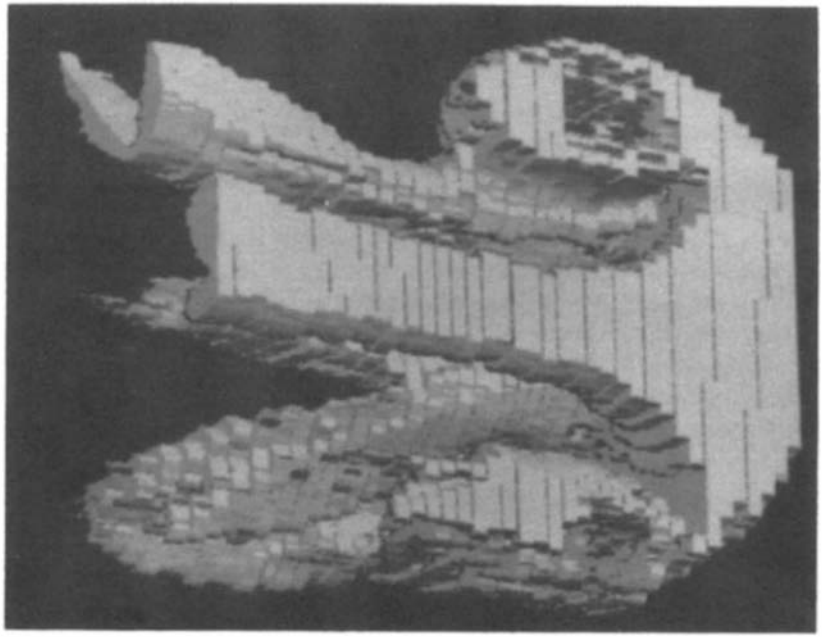

Figure 13 Cross-sectional view of coflowing jet eddy.

can be combined to give dramatic displays as illustrated in the following examples.

5.3.3 DYNAMIC DISPLAY OF STACKED CONTOURS The effectiveness of interactively controlled motion as a depth cue depends on the speed with which projection images can be computed. Observers perceive continuous motion if at least 30 images per second can be generated. Calculating images at even a fraction of this rate limits objects to simple forms and requires special-purpose hardware.

Therefore, a simple three-dimensional representation must be used if motion is to be applied to the display of fluid-flow fields. Another consideration is that fluid flows contain complex inner structures. So, some form of transparency is necessary to allow visualization of these structures. These ideas suggest that the data should be reduced as much as possible to elementary primitives that can be rotated quickly and permit inner structures to be seen.

This reconstruction method creates a set of stacked contour loops. Each two-dimensional cross-sectional image is processed to extract the features of interest (Wu & Hesselink 1987) and is then passed through thresholding and edge-extraction operations. Thus, each processed cross-section finally

consists of one or more closed-loop contours. The contours could be represented as cubic curve segments, line segments, or points. Points are the easiest to handle. They are also more flexible than the other two primitives because a fraction of them can be randomly selected for display to make inner structures more visible.

A three-dimensional representation of the flow field is obtained by stacking the contours in the proper sequence using a constant separation distance between cross-sectional planes. Motion is combined with color encoding and stereopsis to enhance the depth cues. Displays of the stacked contours are generated on a graphics workstation having special hardware that performs three-dimensional perspective, viewing, and modeling transformations, plus three-dimensional clipping.

Stereopsis and color coding produce strong depth cues in these end views, even without motion. The effect is strongest where structures are aligned along the axis of the flow. The connectivity of structures is evident in Figure 14, where the representation uses the full set of points on the contours. By using a smaller number of points we can increase transparency.

The major shortcoming of this method is that the connectivity relationships between structures are difficult to perceive—particularly in views

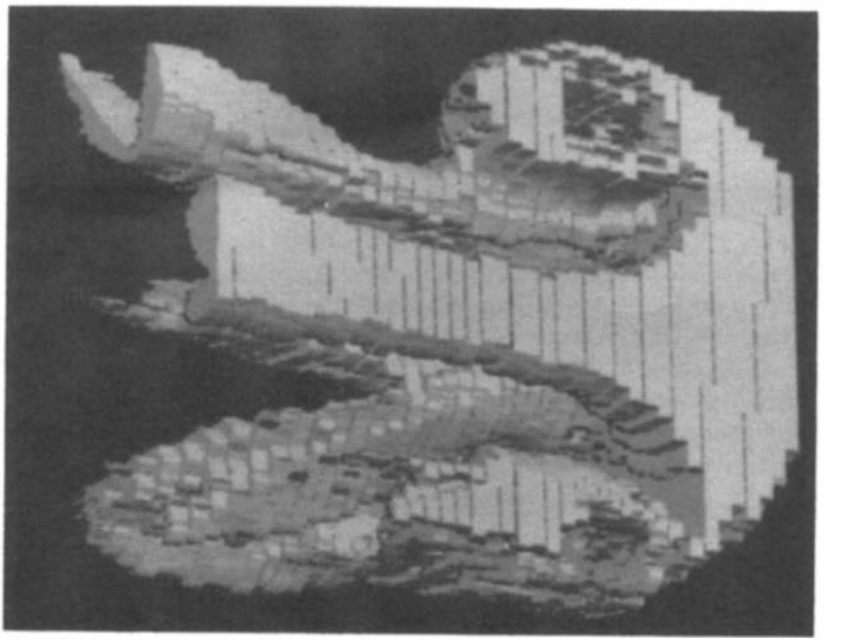

Figure 14 End view of coflowing jet represented as stacked contour loops.

other than the end views. The following method is motivated by the goal of obtaining a better understanding of how structures are connected.

5.3.4 SURFACE RENDITION OF THREE-DIMENSIONAL SCALAR FELDS Clark (1981) proposed an algorithm for the display of pressure contour surfaces of numerical solutions to fluid-flow problems. His method, which is an extension of Catmull's (1974) algorithm for computer display of curved surfaces, uses cubic splines to interpolate scalar quantities in the space between discrete solution points from which surfaces of constant scalar value are then determined. This algorithm can be used for the generation of surfaces from any continuous scalar quantity that is known at points on a rectilinear grid.

Wu & Hesselink (1987) implemented this algorithm and applied it to the display of the full set as well as a smaller subset of the experimental data from the coflowing jet (Agui & Hesselink 1987). Results of this display method are shown in Figures 16–18. The region selected corresponds to the interaction zone between the ring vortex and a longitudinal streamer. A sequence of images representing this portion of the jet structure are shown in Figure 15. A total of 40 images like these make up the original data base. The depth cues used in Figures 16 and 17 are perspective projection, surface shading, hidden-surface removal, and stereopsis. The sensation of depth is very strong. The connectivity and spatial relationships of outer structures are immediately apparent in images reconstructed and displayed with this technique. Care must be taken, however, to interpret the rendered images—in particular, the significance of the detailed surface structure. The shape of the structure can change significantly depending on the interpolation technique used.

5.3.5 DISPLAY WITH PEELING The interior detail of the structures is obscured by hidden-surface removal and the opaque outer shell. In many cases of interest, the topology of interior structures is of interest; in such cases, these structures can be revealed by selectively removing outer layers. For example, inner structures of the interaction region of two vortices are visualized in Figure 18 by peeling outer layers away. This peeling procedure is most useful in an interactive mode under cursor control of a graphics display.

Stereoscopic display after surface peeling provides an extremely powerful tool for analysis of complicated data fields. All the advantages of the surface-rendering technique are preserved, and interior structure can be seen with strong three-dimensional depth cues. Since the human visual system is best adapted to perception of surfaces, a display system that depicts surfaces is inherently easier to comprehend than the semi-transparent renditions of Figure 14. Surface renditions are also much more

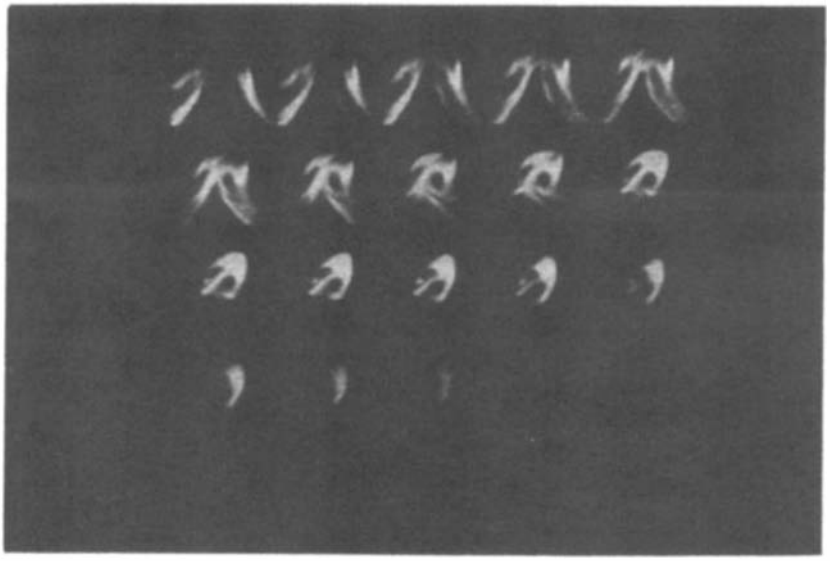

Figure 15 Sequence of digital images comprising a subset of the jet flow shown in Figure 12.

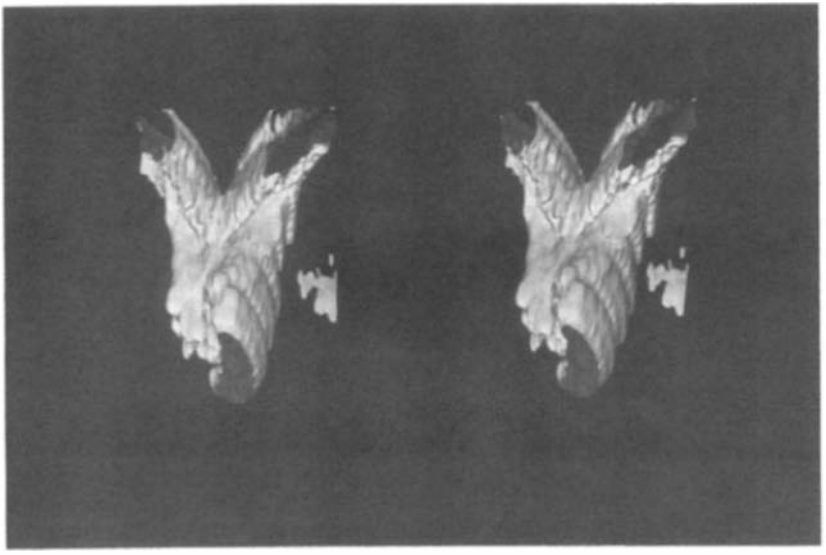

Figure 16 Stereo-pair smooth surface (*C*-spline) rendition of interaction between a longitudinal and ring vortex in coflowing jet. (A simple stereoscope may be used to facilitate fusing the images.)

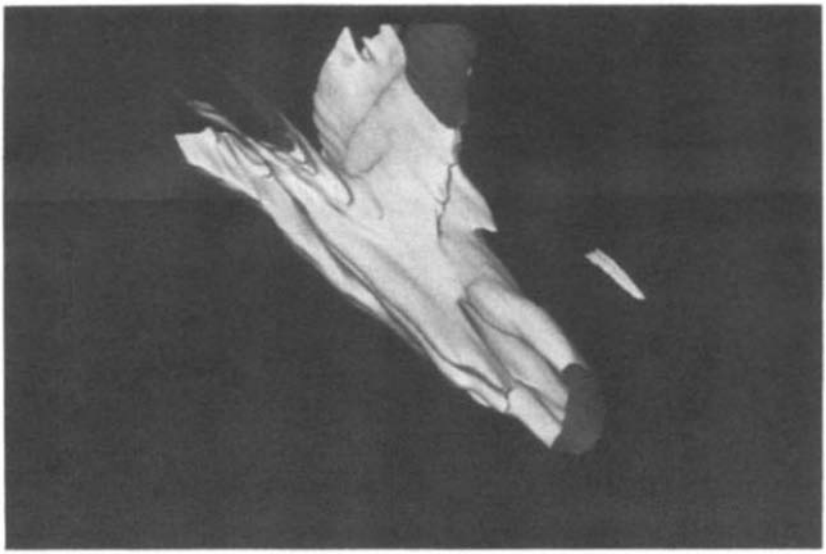

Figure 17 Cubic *B*-spline contour surface of a longitudinal vortical structure in a coflowing jet.

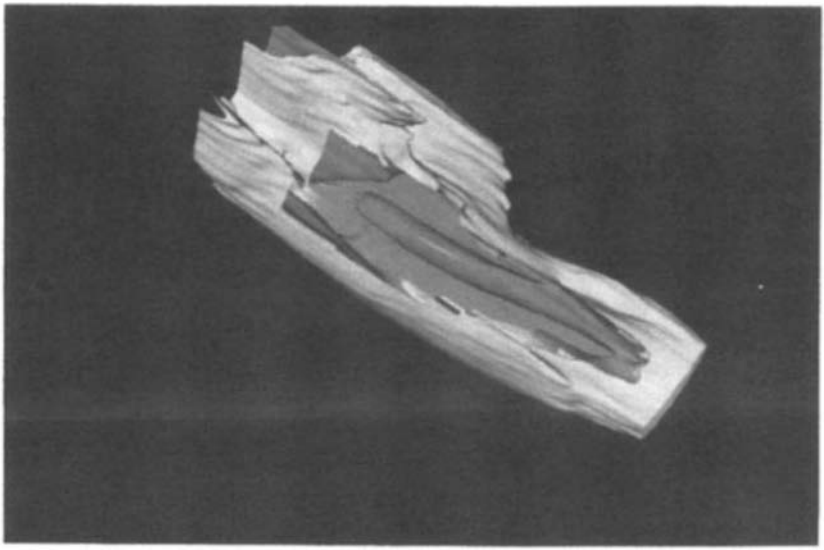

Figure 18 Display of interior detail of Figure 16 by removing outer layers.

effective for data interpretation than are semitransparent displays, which often tend to become rather confusing for complicated data fields.

5.3.6 HOLOGRAPHIC DISPLAYS Three-dimensional experimental and numerically generated data sets can be displayed very effectively using holography. Holographic methods are powerful in the sense that the information stored in a two-dimensional format provides very strong three-dimensional depth cues. Applications of holographic display techniques to flow imagery may be found in Hesselink et al. (1985).

A computational procedure is used to determine views of the object as seen by an observer located some distance away from the object, which in this case is defined by an ordered array of planes. The intensity of light propagating along rays which converge at the eyes of the observer is computed by considering each point in the object to act both as a source and as an attenuator. Each point along the lines, as shown in Figure 19, acts as a source of light and as an attenuator for light coming from points farther away from the observer. The net result of summing all these contributions is the intensity as measured along each ray reaching the observer. The collection of rays corresponding to a particular viewing position is called a projection and represents the view of the object as perceived by the observer from that direction. To generate a wide field of view, projections are computed at 1/3° intervals, and thus for a 120° viewing angle 360 projections are needed. Labels and other numerical data can be added to the data base and made visible in the same fashion.

Upon calculation of the projections, a hologram is created by using an arrangement as shown in Figure 20. Each computed projection is displayed on a flat CRT screen and recorded in sequence on a 16-mm movie, which results in 360 movie frames, each representing one projection. The images are recorded holographically using an anamorphic imaging stystem. A laser illuminates one frame, and a combination of a spherical and a cylindrical lens images the projection onto a narrow slit in front of holographic film. Simultaneously, a reference beam is derived from the same laser and a hologram is recorded on the film, one strip hologram for each

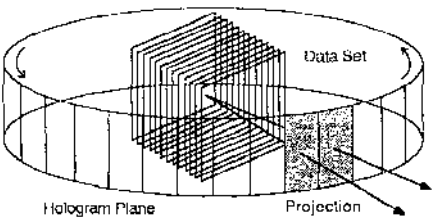

Figure 19 Source-attenuation model for computing projections.

Holographic representation of a co-flowing jet eddy.
(From Agui & Hesselink 1987, and Wu & Hesselink 1987)

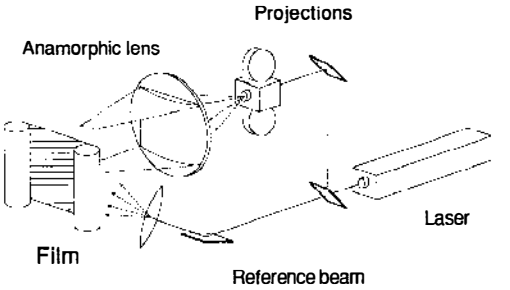

Figure 20 Holographic recording of projection in a multiplex hologram.

projection for a total of 360 holograms side by side. The hologram may be viewed by wrapping the film around a cylinder for large field of view displays or by placing it on a flat substrate and using a point light source as shown in Figure 21; for this purpose a white-light source is adequate. The object appears to be present behind the film and can be viewed by an observer located on the other side of the hologram. The procedure described here creates distortions for objects large compared with the enclosed volume of the cylindrical hologram and for large viewing angles; these distortions can be compensated for by properly modifying the data base before calculating the projections (Jaffey et al. 1984).

For the purpose of displaying the data in publishable form, yet another transformation is needed. The hologram as described here is used as a

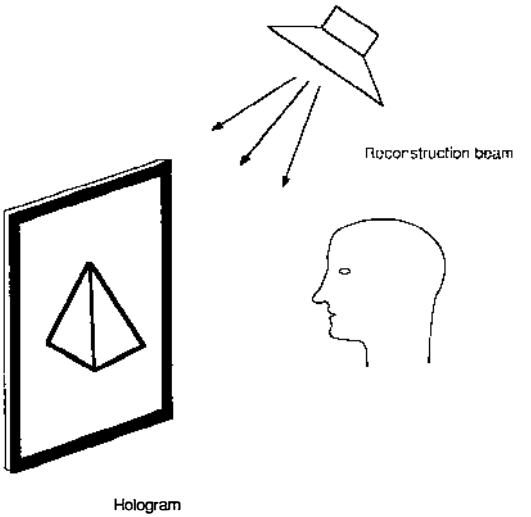

Figure 21 Viewing configuration for a multiplex hologram.

master from which embossed or photopolymer copies are made using standard holographic techniques (Caulfield 1979). This procedure produces a reflection hologram, in which the image is located relatively close to the hologram plane and often straddles it. Such a hologram (see the holographic insert) can be viewed using white light.

With this technique it is possible to display time-varying three-dimensional objects in animated form. Besides displaying different views of the same static object, one can show a time sequence so that time is encoded in angular position. Thus it is possible to display four-dimensional data.

Comprehension of complicated three-dimensional data—even when using the powerful techniques described here—may be beyond the capabilities of the human visual system. In this case the data set needs to be simplified, which may be accomplished by image decomposition.

5.3.7 AUTOMATED IMAGE ANALYSIS The well-established field of automated scene analysis can provide some useful analogies for the development of automated flow analysis, especially in the definition of an abstract representation of a "scene" consisting of objects, their characteristics, and relationships. But the differences in the form of the data (a continuous vector field vs. a discontinuous scalar image) and the a priori knowledge (differential equations vs. contextual relationships) make the problem of recognizing patterns and structures in original data very different. In the study of fluid-flow data, it is necessary to determine the topological structures in the flow from a continuous vector field that has no well-defined boundaries between structures. One way of doing this is through the analysis of critical points (Perry & Chong 1987). In particular, critical-point analysis combined with digital image processing may prove to be a powerful approach for automated flow analysis and for comparison between similar three-dimensional data sets.

Hesselink & Helman (1987) advocate the development of a scene-like representation of the flow topology using local features as a basis. This reduces the problem to one of synthesizing the features located by local analysis into a representation of the global topology of the flow and doing so in an automated fashion. In principle, one could carry out a Taylor-series expansion to a sufficiently high order as to fully characterize the flow. But this could be computationally very intensive; for example, a fifth-order expansion in three dimensions requires the determination of 168 coefficients and would still not yield results that could be readily interpreted. Instead of going to high-order expansions, we compute the local characteristics of the critical points in the flow and then determine the connecting streamlines and surfaces by integrating the velocity field. The topology of the flow can then be reduced to a graph with these structures

represented as nodes and their relationships in the flow as the connecting lines of the graph. Once the data field has been placed in this form, it may be studied and compared with other data sets using techniques from syntactic pattern recognition or displayed using shaded surfaces.

There are several problems that must be solved for this approach to be successful. First, a system is required for the abstract representation of structures in the flow and the connections between them in all their variety and complexity. Second, recognition algorithms need to be developed to extract this abstract representation from the input data. And lastly, techniques are required for the display of the representation in an intelligible manner.

Image decomposition of three-dimensional flows may proceed by using a finite number of flow patterns that can be deduced for the description and analysis of flow fields (Kaplan 1958, Monorski 1962). These patterns can be identified in two-dimensional planes—often exhibiting symmetry—and can provide a framework for classification of the flow, even outside the plane containing the critical points. This reduced data set may then be used for data-base comparison.

Comparison of data sets is a difficult task when working directly with the raw data, since a change in the position of a structure may, without altering the basic topology of the flow, significantly change the values of the vector field at corresponding grid points. Since the graph is unique to the topology of the flow, it can be used as a basis for comparing different data sets. If the topologies are the same, the graphs will be as well, and hence positions of structures, principal directions of critical points, and the shapes of the flows within segments can all be readily compared between the flow fields by examining the quantitative attributes stored in the representation on a node-by-node basis.

5.3.8 COMPARING TOPOLOGICALLY DIFFERENT DATA SETS A grammar of graphs can be defined to describe the allowed orders in which nodes may be connected (Hsu et al. 1978, Gonzales & Thomason 1978). The set of all possible flow fields is the set of all sentences in a language, and the grammar a set of rules that generates them. Within this framework, rewriting rules can be defined that replace a certain subgraph with another subgraph (Hesselink & Helman 1987).

As an example, consider the two-dimensional flow over three rotating cylinders shown in Figure 22 and the corresponding graph shown in Figure 23. By increasing the circulation of the cylinder in the upper right-hand corner of Figure 22, the graph is modified as shown in Figure 24. This is an actual change in the topology of the flow, since it implies that there is some fluid passing over the left cylinder that will pass under the right cylinder. This is a very different representation.

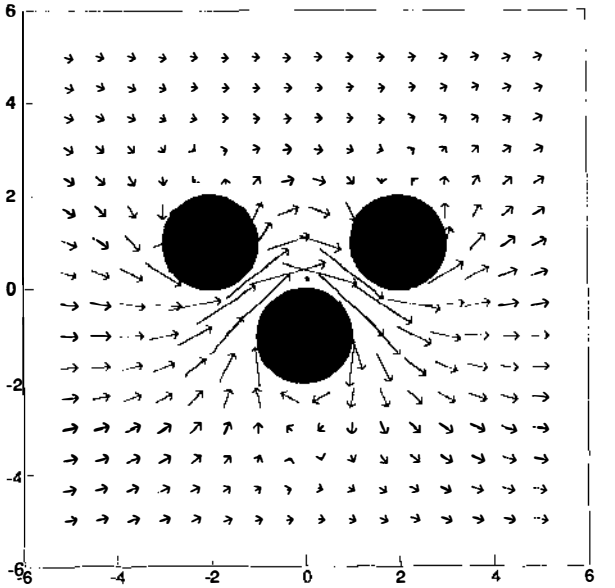

Figure 22 Sample velocity field. Ideal flow around rotating cylinders.

If the topologies are different, we are no longer able to directly compare the representations depicted in Figures 23 and 24, but if the topologies are similar, it might be possible to transform one into the other using replacement rules. A grammar of graphs can be defined to describe the allowed orders in which nodes may be connected (Gonzales & Thomason 1978). For example, the rule shown in Figure 25 is capable of transforming the graph in Figure 23 into that in Figure 24. Although it would be very difficult to maintain the quantitative information stored in the nodes of the graph across such a rewriting, determining the minimum number of rewriting rules required to transform the topology of one flow field into that of another would provide a useful way of characterizing the topological differences between data sets. The approach can be generalized to three dimensions, where the structures of interest include three-dimensional critical points, lines of two-dimensional critical points, bifurcation lines, and the streamlines and surfaces that connect them.

5.3.9 EVALUATION To visualize complicated three-dimensional flow structures, one requires displays with strong three-dimensional depth cues. From experience, we have found that rendering of opaque or semi-transparent surfaces (such as the interface between two fluids or a contour

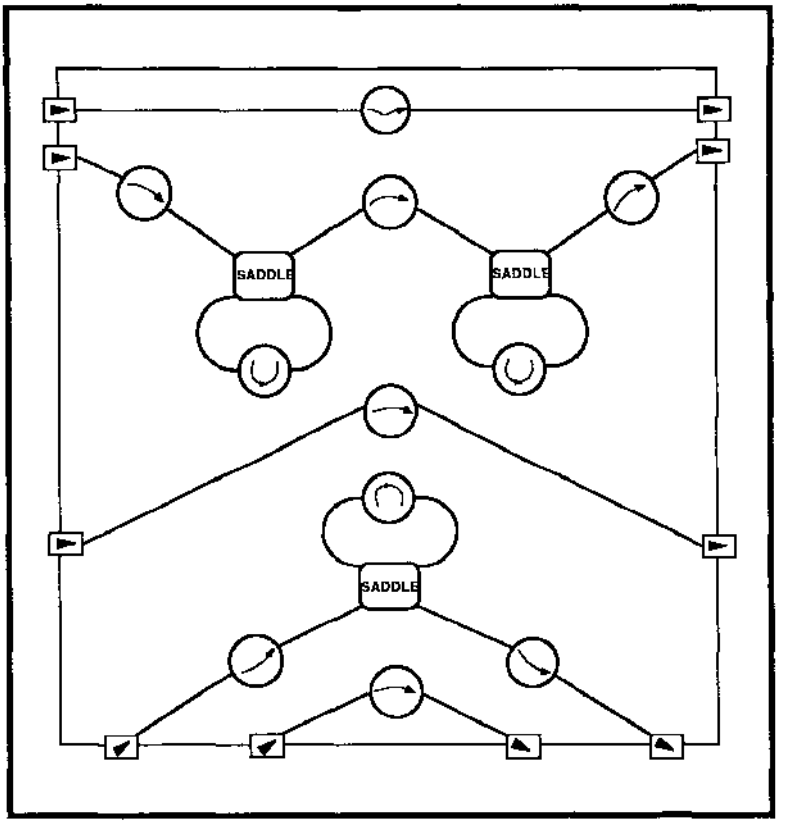

Figure 23 Graph depiction of representation of rotating-cylinder flow.

surface) provides the best results. In particular, when combined with an interactive surface-peeling capability for examination of interior flow detail, surface rendering is preferable over displays of stacked contours or dot patterns. Alternatively, the source-attenuation method provides transparency and is relatively easily implemented, but at the expense of strong depth cues; fluid flows tend to look like clouds unless interfaces or other surfaces are accentuated. This method, however, is useful for display of data with inherently strong boundaries between flow regions, such as may be obtained with recording of fluorescence in liquid flows, where diffusion does not blur sharp edges. Numerically generated binary data such as three-dimensional stream and contour lines may also be displayed with good results. Additionally, the attenuation coefficient can be made so large that only outer surfaces are rendered visible.

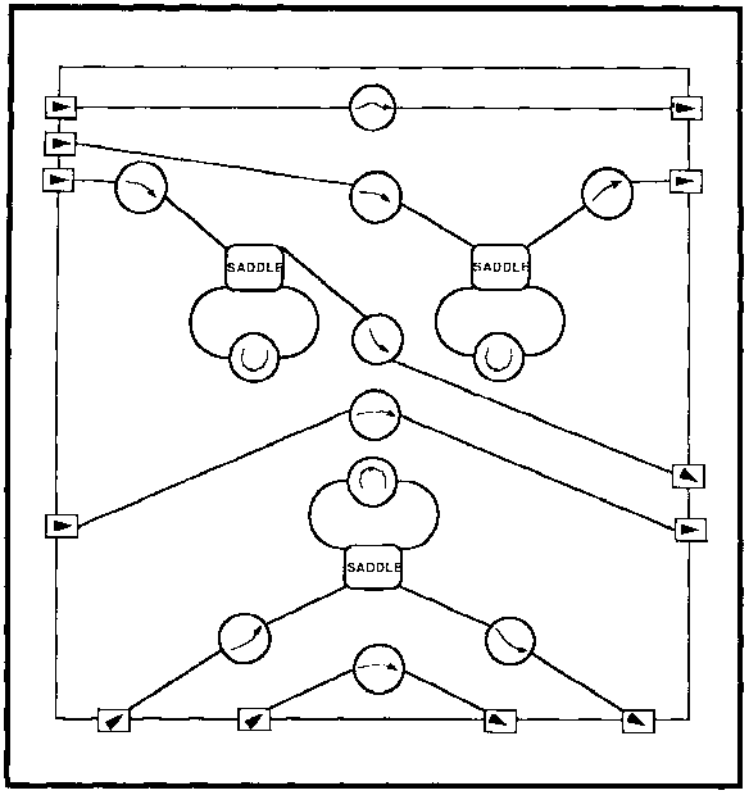

Figure 24 Graph representation of modified flow.

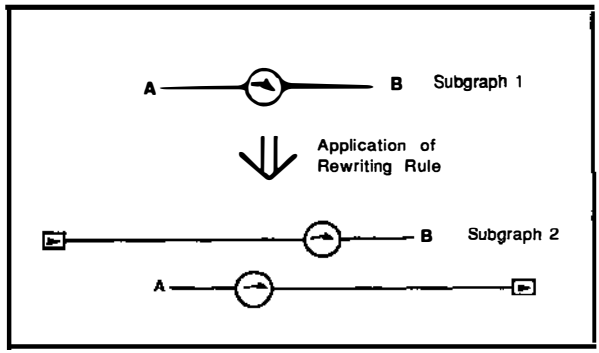

Figure 25 Example of a rewriting rule.

To provide three-dimensional depth cues, stereo is preferable over motion parallax because it allows detailed observation of structure in a stationary image. Motion parallax, on the other hand, provides three-dimensional depth cues, but topological details cannot be studied leisurely; the object is always moving. For certain simple flows this may be acceptable and useful, but for complicated intricate objects this approach is less than satisfactory. The ability to rotate objects, preferable under cursor control, however, is desirable, in particular when combined with stereopsis, shading, hidden surface removal, and surface-peeling capabilities. As a general rule, the more complicated the object, the more numerous and stronger the depth cues needed to render the object visible; a combination of approaches then provides the best results. In this regard, surface shading, texture, and illumination schemes provide complementary depth cues, albeit at the expense of increased computational burden. For example, a small amount of texture in the form of random dot patterns or noise superimposed on surface displays with shading can provide excellent depth cues. As an additional attribute, color enhancement is also useful to enhance depth cues in the form of intensity or range encoding.

Although these three-dimensional representations can be very powerful, they do not always provide good results. For example, in general, scalar data sets are much more effectively rendered than vector fields, because at every point in space we need to display both a magnitude and a direction. Even displays of small sets of vectors, on the order of a few hundred in a volume of a few centimeters on a side, are often too confusing to be useful, even when presented with stereo and additional depth cues. Motion parallax of vector data is by itself almost always inadequate, even for simple flows. Similarly, it is better to display particle traces with three-dimensional depth cues than vectors. But even in that case, when the concentration of traces is high (usually more than a few dozen) and the traces are in close proximity, the display becomes confusing and it is necessary to rotate, magnify, or simplify the object to discern its structure. Alternatively, velocity ribbons or isovelocity surfaces may be displayed more effectively than particle traces.

Even when using the most sophisticated display attributes presently available, our visual system is often not powerful enough for analysis of complex flow topologies. Clearly, new approaches need to be developed to reduce the information content yet retain all essential topological features. One approach to data compaction is automated image decomposition in terms of critical points and connecting lines or surfaces. In this approach, velocity fields are represented by elementary structures and their connections, which may be displayed using powerful surface-rendering techniques. From the representation the velocity field can still be

computed, but the difficulties with displaying and analyzing the vector field for determining flow topology are avoided. In addition, elementary decomposition techniques may be combined with syntactic image-processing approaches to provide a very effective framework for three-dimensional data analysis and comparison. This approach, we believe, is preferable over direct display of vectorial data. Although decomposition into elementary structures can be computationally intensive for complex three-dimensional flows, without such a data compaction both quantitative and qualitative data analysis of large data sets are very difficult.

Most of the techniques described in this section can be implemented with video technology interfaced to computers. Such systems allow flexibility and interactive processing, which is particularly useful when monitoring results or progress of large-scale numerical flow simulations. On the other hand, fast interactive response requires powerful graphics systems when dealing with complicated flows. Alternatively, holography can provide strong depth cues including motion parallax and stereopsis, and shading, texture, and even color can be brought to bear to render the object visible. At present, however, holography is not an interactive display medium because generation of computer-assisted holograms of a large enough size to have a good field of view is still too large a task for even the fastest computers available today. In addition, real-time recording devices suitable for display holograms are not yet available. Thus, for interactive display of three-dimensional imagery, video-based systems are still preferable over holographic devices. For archival purposes, however, holography can be an excellent display medium. For example, embossed reflection holograms can be mass produced and images may be rendered visible with an incandescent light source. It appears, in particular for educational purposes, that holograms can be used effectively to display complex three-dimensional flow structures with excellent depth cues and quality.

6. CONCLUDING REMARKS

The use of digital computers greatly enhances the usefulness of flow-visualization techniques. Classical methods are improved and quantitative information can be extracted from optical techniques that previously provided only qualitative data. In addition, a whole new class of imaging techniques has been developed. The most striking and promising of these techniques are optical tomography and gradient imaging, which allow the interior of flows to be probed and visualized using line-of-sight techniques applied from different directions.

On the other hand, sheet-illumination techniques provide powerful means to visualize the interior of flows. Particle tracking is an intuitively attractive method for making velocity measurements, but care should be exercised when attempting to determine derivative data. It is well known that numerical differentiation is a process prone to large errors, particularly when the velocity field is only available on a randomly spaced grid. Some of these error sources may be reduced by seeding the flow more densely and using optical processors to determine velocity on a regular grid, as described in the section on speckle velocimetry.

Digital techniques allow enhancement and feature extraction of images to assist data interpretation of both numerical and experimental data. Recent advancements in computer-assisted data acquisition, development of sophisticated optical techniques, and increasing power and speed of computers for numerical analysis of flows provide ever-increasing sizes of data sets. These data, representing three-dimensional time-evolving flows, are too complicated to be interpreted and evaluated by visual inspection alone. Data-base comparison and feature extraction need to be automated using such techniques as critical-point analysis and automated image decomposition.

Digital image processing thus provides exciting new diagnostics for visualization and quantitative analysis of both experimental data and numerically computed flows. Ultimately, automated processing may allow complicated data sets to be analyzed, dissected, and represented in terms of simplified graphs. These representations may be sufficiently rich to uniquely describe complicated multi-dimensional flows and yet be simple enough to allow meaningful comparisons between different data sets using syntactic rules. This approach is still in its infancy but appears to be promising.

The effort devoted to image understanding requires substantial resources and may soon become comparable or even larger than the one required to generate the data. Moreover, flow visualization will no longer be exclusively in the domain of experiments, but will also play a significant role for evaluation and interpretation of computed flows.

ACKNOWLEDGMENTS

It is a pleasure to acknowledge my students for their research accomplishments, friendship, and stimulating interactions. This work was supported by DOE under contract DE-FG03-85ER13312 and by NSF under contract NSF ECS 84-17869.

Literature Cited

Adrian, R. J. 1986. Multi-point optical measurements of simultaneous vectors in unsteady flow—a review. *Int. J. Heat Fluid Flow* 7(2): 127–45

Agui, J. C., Jiménez, J. 1987. On the performance of particle tracking. *J. Fluid Mech.* In press

Agui, J. C., Hesselink, L. 1987. Flow visualization and numerical analysis of a coflowing jet: a three-dimensional approach. *J. Fluid Mech.* In press

Alden, M., Schawlow, A. L., Svanberg, S., Wendt, W., Zliang, P. L. 1984a. Three-photon-excited fluorescence detection of atomic hydrogen in an atmospheric pressure flame. *Opt. Lett.* 9: 211–13

Alden, M., Wallin, S., Wendt, W. 1984b. Applications of two-photon absorption for detection of CO in combustion gases. *Appl. Phys. B* 33: 205–8

Aldcn, M., Hertz, H. M., Svanberg, S., Wallin, S. 1984c. Imaging laser-induced fluorescence of oxygen atoms in a flame. *Appl. Opt.* 23(19): 3255–57

Alwang, W. L., Cavanaugh, L., Burr, R., Hauer, A. 1970. Some applications of holographic interferometry to analysis of the vibrational response of turbine engine components. *Tech. Rep. A70-33134*, Electro-Opt. Syst. Des. Conf., New York, NY

Andrew, H. C., Hunt, B. R. 1978. *Image Restoration.* New York: Academic

Arcelli, C., Cordella, L., Levialdi, S. 1975. Parallel thinning of binary pictures. *Electron. Lett.* 11: 148–49

Arnold, W., Hinsch, K., Platen, W. 1986. Analysis of non-stationary flows by evaluating the fringe visibility in speckle velocimetry. *Proc. Int. Symp. Flow Visualization, 4th, Paris*, pp. 127–32. Washington, DC: Hemisphere

Augustyn, W. 1979. Versatility of microprocessor based interferometric reduction system. *Proc. Soc. Photo-Opt. Instrum. Eng.* 192: 128–33

Barrett, H., Swindell, W. 1981. *Radiologic Imaging.* New York: Academic

Becker, F., Meier, G. E. A., Wegner, H. 1982. Automatic evaluation of interferograms. *Proc. Soc. Photo-Opt. Instrum. Eng.* 259: 386–93

Bennett, K., Byer, R. L. 1984. Optical tomography: experimental verification of noise theory. *Opt. Lett.* 9: 270–72

Bennett, K. E., Faris, G. W., Byer, R. L. 1984. Experimental optical fan beam tomography. *Appl. Opt.* 23: 2678–85

Bennett, K. E., Byer, R. L. 1986. Fan-beam-tomography noise theory. *J. Opt. Soc. Am. A* 3(5): 624–33

Bernal, E., Loomis, J. 1977. Interactive video image digitizer—application to interferogram analysis. *Proc. Soc. Photo-Opt. Instrum. Eng.* 126: 143–51

Biscos, Y., Bismes, F., Hebrard, P., Lavergne, G., Toulouse, G. 1986. Digital video image processing applications to drop size and concentration measurements. *Proc. Int. Symp. Flow Visualization, 4th, Paris*, pp. 253–59. Washington, DC: Hemisphere

Bracewell, R. N. 1956. Strip integration in radio astronomy. *Aust. J. Phys.* 9: 198–217

Brown, G. L., Roshko, A. 1974. On density effect and large structure in turbulent mixing layers. *J. Fluid Mech.* 64: 775–816

Button, B. L., Cutts, J., Dobins, B. N., Moxon, C. J., Wykes, C. 1985. The identification of fringe positions in speckle patterns. *Opt. Laser Technol.* 17: 189–92

Byer, R. L., Shepp, L. A. 1979. Two-dimensional remote air pollution monitoring by tomography. *Opt. Lett.* 4: 75–77

Castleman, K. R. 1979. *Digital Image Processing.* Englewood Cliffs, NJ: Prentice-Hall

Catmull, E. 1974. A subdivision algorithm for computer display of curved surfaces. *Tech. Rep. UTEC-CSc-74-133*, Univ. Utah, Salt Lake City

Caulfield, H. J. 1979. *Handbook of Optical Holography.* New York: Academic

Cha, S., Vest, C. M. 1979. Interferometry and reconstruction of strongly refracting asymmetric-refractive-index fields. *Opt. Lett.* 4: 311–13

Cha, S., Vest, C. M. 1981. Tomographic reconstruction of strongly refracting fields and its application to interferometric measurement of boundary layers. *Appl. Opt.* 20(16): 2787–94

Chang, T. P., Wilcox, N. A., Tatterson, G. B. 1984. Application of image processing to the analysis of three-dimensional flow fields. *Opt. Eng.* 23(3): 283–87

Cheng, S., Zimmermann, M., Miles, R. B. 1983. Supersonic-nitrogen flow-field measurements with the resonant Doppler velocimeter. *Appl. Phys. Lett.* 43(2): 143–45

Choudry, A. 1981. Digital holographic interferometry of convective heat transport. *Appl. Opt.* 20: 1240–44

Clark, J. H. 1981. Parametric curves, surfaces and volumes in computer graphics and computer-aided geometric design. *Tech. Rep. 221*, Comput. Syst. Lab., Stanford Univ., Calif.

Cline, H. E., Holik, A. S., Lorensen, W. E. 1982. Computer aided surface reconstruction of interference contours. *Appl. Opt.* 21: 4481–88

Collicott, S., Hesselink, L. 1986. Anamorphic optical processing of multiple-exposure speckle photographs. *Opt. Lett.* 11: 410–12

Collicott, S., Hesselink, L. 1987. Real time speckle velocimetry with recording in photorefractive crystals. *AIAA Pap. No. 87-1376*

Corke, T. C. 1981. *A new view on origin, role and manipulation of large scales in turbulent boundary layers.* PhD thesis. Ill. Inst. Technol., Chicago

Corke, T. C. 1983. Two-dimensional match filtering as a means of image enhancement in visualized turbulent boundary layers. *AIAA Pap. No. 83-0379*

Crowder, J. P., Beck, H. N. 1985. Electronic wake imaging systems. *Proc. Int. Symp. Flow Visualization, 3rd, 1983*, pp. 715–19. Washington, DC: Hemisphere

Dainty, J. C. 1975. Laser speckle and related phenomena. *Top. Appl. Phys.* 9: 1

Dändliker, R. 1980. Heterodyne holographic interferometry. In *Progress in Optics*, ed. E. Wolf, 17: 1–84. Amsterdam: North-Holland

Dändliker, R., Thalmann, R. 1983. Determination of 3-D displacement and strain by holographic interferometry for non-plane objects. *Proc. Soc. Photo-Opt. Instrum. Eng.* 398: 11–16

Dändliker, R., Thalmann, R. 1987. Electronic processing for holographic interferometry. In *Optical Metrology*, pp. 426–40. The Hague, Neth: Nijhoff

Dändliker, R., Thalmann, R., Willemin, J. F. 1982. Fringe interpolation by two-reference-beam holographic interferometry: reducing sensitivity to hologram misalignment. *Opt. Commun.* 42: 301–6

Dändliker, R., Weiss, K. 1970. Reconstruction of the three-dimensional refractive index from scattered waves. *Opt. Commun.* 1: 323–28

Devaney, A. J. 1983. A computer simulation study of diffraction tomography. *IEEE Trans. Biomed. Eng.* 30(7): 377–86

Dimotakis, P. E., Debussy, F. D., Koochesfahani, M. M. 1981. Particle streak velocity field measurements in a two-dimensional mixing layer. *Phys. Fluids* 24(6): 995–99

Dines, K. A., Lytle, R. J. 1979. Computerized geophysical tomography. *Proc. IEEE* 67(7): 1065–73

Durst, F., Melling, A., Whitelaw, J. H. 1976. *Principles and Practice of Laser-Doppler Anemometry.* London: Academic. 412 pp.

Emmerman, P. J., Goulard, R., Santoro, R. J., Semerjian, H. G. 1980. Multiangular absorption diagnostics of a turbulent argon-methane jet. *J. Energy* 4: 70–77

Erbeck, R. 1985. Fast image processing with a microcomputer applied to speckle photography. *Appl. Opt.* 24(22): 3838–41

Faris, G. W., Byer, R. L. 1986. Quantitative optical tomography imaging of a supersonic jet. *Opt. Lett.* 11: 413–15

Foley, J. D., Van Dam, A. 1982. *Fundamentals of Interactive Computer Graphics.* Reading, Mass: Addison-Wesley

Frieden, B. R., Zoltani, C. K. 1985. Maximum bounded entropy: application to tomography reconstruction. *Appl. Opt.* 24(23): 3993–99

Funnell, W. R. J. 1981. Image processing applied to the interactive analysis of interferometric fringes. *Appl. Opt.* 20: 3245–49

Fusch, H., Zedem, Z. M., Uselton, S. P. 1977. Optimal reconstructions from planar contours. *Commun. ACM* 20: 693–702

Gennero, C., Mathe, J. M. 1985. Real time edge extraction application to the study of vortices cores. *Proc. Int. Symp. Flow Visualization, 3rd, 1983*, pp. 418–22. Washington, DC: Hemisphere

Gharib, M., Hernan, M. A., Yavrouian, A. H., Sarohia, V. 1985. Flow velocity measurement by image processing of optically activated tracers. *AIAA Pap. No. 85-0172*

Gilbert, P. 1972. Iterative methods for the three-dimensional reconstruction of an object from projections. *J. Theor. Biol.* 36: 105–17

Goldsmith, J. E. M., Anderson, R. J. M. 1985. Imaging of atomic hydrogen in flames with two-step saturated fluorescence detection. *Appl. Opt.* 24(5): 607–9

Gonzales, R. C., Thomason, M. G. 1978. *Syntactic Image Processing.* Reading, Mass: Addison-Wesley

Goodman, J. W. 1985. *Statistical Optics.* New York: Wiley-Interscience

Gordon, R. 1974. A tutorial on art (algebraic reconstruction techniques). *IEEE Trans. Nucl. Sci.* 21: 78–93

Goulard, R. 1976. Optical measurements of thermodynamic properties in flow fields. *AGARD-CP-193*, Pap. 13

Grishin, M. P., Kurbanov, S. M., Markelov, V. P., Sokolov, V. A. 1974. Some aspects in the analysis of interference patterns using digital computers. *J. Appl. Spectrosc.* 20: 517–22

Hasen, G., Graham, J. 1985. Computer generated graphics display of Navier-Stokes flow solutions. *Proc. Int. Symp. Flow Visualization, 3rd, 1983*, pp. 645–49. Washington, DC: Hemisphere

Haussmann, G., Lauterborn, W. 1980. Determination of size and position of fast moving gas bubbles in liquids by digital 3-D image processing of hologram reconstruction. *Appl. Opt.* 19(20): 3529–35

Herman, G. T., ed. 1979. *Image Reconstruction From Projections. Implementation and Applications.* Berlin: Springer-Verlag. 284 pp.
Herman, M., Kanade, T. 1986. The 3-D mosaic scene understanding system. In *From Pixels to Predicates: Recent Advances in Computational and Robotic Vision*, pp. 322–58. Norwood, NJ: Ablex
Hernan, M. A., Parikh, P., Sarohia, V. 1985. Digital image processing application to spray and flammability studies. *Proc. Int. Symp. Flow Visualization, 3rd, 1983*, pp. 402–6. Washington, DC: Hemisphere
Hertz, H. M. 1985. Experimental determination of 2-D flame temperature fields by interferometric tomography. *Opt. Commun.* 54: 131–36
Hertz, H. M. 1986. Kerr effect tomography for nonintrusive, spatially resolved measurements of asymmetric electric field distributions. *Appl. Opt.* 25: 914–21
Hesselink, L. 1987a. Optical processing of images. In *Handbook of Flow Visualization.* Washington, DC: Hemisphere
Hesselink, L. 1987b. Optical tomography. In *Handbook of Flow Visualization.* Washington, DC: Hemisphere
Hesselink, L., Helman, J. 1987. Evaluation of flow topology from numerical data. *AIAA Invited Pap.: 87-1181-CP*
Hesselink, L., Pender, J., Jaffey, S., Dutta, K. 1985. Quantitative three-dimensional flow visualization. In *Proc. Int. Symp. Flow Visualization, 3rd, 1983*, pp. 375–80. Washington, DC: Hemisphere
Hesselink, L., White, B. S. 1983. Digital image processing of flow visualization photographs. *Appl. Opt.* 22(10): 1454–61
Hinsch, K., Schipper, W., Mach, D. 1984. Fringe visibility in speckle velocimetry and the analysis of random flow components. *Appl. Opt.* 23(24): 4460–62
Hsu, S., Mundy, J. L., Beaudet, P. R. 1978. Web representation of image data. *Proc. Int. Joint Conf. Pattern Recognition, 4th*, pp. 675–80. Kyoto, Jpn: IEEE Comput. Soc.
Huntley, J. M. 1986. Speckle photography fringe analysis by the Walsh transform. *Appl. Opt.* 25(3): 382–85
Imaichi, K., Ohmi, K. 1983. Numerical processing of flow-visualization pictures—measurement of two-dimensional vortex flow. *J. Fluid Mech.* 129: 283–311
Ineichen, B., Eglin, P., Dändliker, R. 1980. Hybrid optical and electronic processing for strain measurements by speckle photography. *Appl. Opt.* 19: 2191–95
Isacson, S. A., Kaufmann, G. H. 1985. Two-dimensional digital processing of speckle photography fringes. 1: Diffraction halo influence for the noise-free case. *Appl. Opt.* 24(2): 189–93
Jaffey, S. M., Dutta, K., Hesselink, L. 1984. Digital reconstruction methods for three-dimensional image visualization. *Proc. Soc. Photo-Opt. Instrum. Eng.* 507: 155–63
Jagota, R. C., Collins, D. J. 1972. Finite fringe holographic interferometry applied to a right circular cone at angle of attack. *J. Appl. Mech.* 39(4): 897–903
Jian, L., Schmitt, F. 1982. Water current determination by picture processing. In *ICASSP 82*, pp. 830–33. Paris: IEEE
Jiménez, J. 1984. Planning an experiment for digital image processing. In *Digital Image Processing in Fluid Dynamics.* Brussels: von Kármán Inst.
Jiménez, J., Gogollos, M., Bernal, L. P. 1985. A perspective view of the plane mixing layer. *J. Fluid Mech.* 152: 125–43
Jones, H. D. 1977. Computer reduction of holographic interferograms. *Tech. Rep. SAND-77-8236*, Sandia Natl. Labs., Albuquerque, N.M.
Kaplan, W. 1958. *Ordinary Differential Equations.* Reading, Mass: Addison-Wesley
Kaufmann, G. H. 1981. Numerical processing of speckle photography data by Fourier transform. *Appl. Opt.* 20(24): 4277–80
Keffer, J. F., Kawall, J. G., Shokr, M. 1985. An image processing technique for determining properties of turbulent flows. *Proc. Int. Symp. Flow Visualization, 3rd, 1983*, pp. 305–9. Washington, DC: Hemisphere
Kent, J. C., Eaton, A. R. 1982. Stereo photography of neutral density He-filled bubbles for 3-D fluid motion studies in an engine cylinder. *Appl. Opt.* 21(5): 904–12
Kimura, I., Takamori, T. 1986. Image processing of flow around a circular cylinder by using correlation technique. *Proc. Int. Symp. Flow Visualization, 4th, Paris*, pp. 221–26. Washington, DC: Hemisphere
Kirchartz, K. R., Muller, U., Oertel, H. Jr., Zierep, J. 1981. Axisymmetric and non-axisymmetric convection in a cylindrical container. *Acta Mech.* 40: 181–94
Kittleson, J. K., Yu, Y. 1985. Transonic rotor flow—measurement technique using holographic interferometry. *J. Am. Helicopter Soc.* 30(4): 3–10
Kobayashi, T., Saga, T., Segawa, S. 1986. Some considerations on automated image processing of pathline photographers. *Rep.*, Inst. Ind. Sci., Univ. Tokyo, Jpn.
Koochesfahani, M. M., Dimotakis, P. E. 1986. Mixing and chemical reactions in a turbulent liquid mixing layer. *J. Fluid Mech.* 170: 83–112
Kosakoski, R. A., Collins, D. J. 1974. Application of holographic interferometry to

density field determination in transonic corner flow. *AIAA J.* 12(6): 767–70

Kreis, T. M., Kreitlow, H. 1979. Quantitative evaluation of holographic interference patterns under image processing aspects. *Proc. Soc. Photo-Opt. Instrum. Eng.* 210: 196–202

Kychakoff, G., Howe, R. D., Hanson, R. K. 1984. Quantitative flow visualization technique for measurements in combustion gases. *Appl. Opt.* 23(5): 704–12

Kychakoff, G., Howe, R. D., Hanson, R. K., McDaniel, J. C. 1982. Quantitative visualization of combustion species in a plane. *Appl. Opt.* 21(18): 3225–29

Lauterborn, W., Vogel, A. 1984. Modern optical techniques in fluid mechanics. *Ann. Rev. Fluid Mech.* 16: 223–44

Lewitt, R. M., Bates, R. H. T. 1978. Image reconstruction from projections: III. Projection completion methods (theory). *Optik* 50: 189–204

Lourenco, L. M. 1986. Speckle velocimetry. In *Digital Image Processing in Fluid Dynamics*. Brussels: von Kármán Inst.

Macovski, A. 1983. *Medical Imaging Systems*. Englewood Cliffs, NJ: Prentice-Hall

Macy, W. W. Jr. 1983. Two-dimensional fringe-pattern analysis. *Appl. Opt.* 22(23): 3898–3901

Maldonado, C. D., Olsen, H. N. 1966. New method for obtaining emission for emitted spectral intensities. II. Asymmetrical sources. *J. Opt. Soc. Am.* 56: 1305–13

Mandella, M. J. 1987. *Experimental and analytical studies of compressible vortices*. PhD thesis. Stanford Univ., Calif.

Marko, K. A., Rimai, L. 1985. Video recording and quantitative analysis of seed particle track images in unsteady flows. *Appl. Opt.* 24(21): 3666–72

Marr, D. 1982. *Vision*. New York: Freeman

Mastin, G. A., Ghiglia, D. C. 1985. Digital extraction of interference fringe contours. *Appl. Opt.* 24(12): 1727–28

Matulka, R. D., Collins, D. J. 1971. Determination of three-dimensional density fields from holographic interferograms. *J. Appl. Phys.* 42: 1109–19

McDaniel, J. C., Hiller, B., Hanson, R. K. 1983. Simultaneous multiple-point velocity measurements using laser-induced iodine fluorescence. *Opt. Lett.* 8(1): 51–53

Mertz, L. 1983. Real-time fringe pattern analysis. *Appl. Opt.* 22: 1535–38

Merzkirch, W. 1974. *Flow Visualization*. New York: Academic. 250 pp.

Meynart, R. 1980. Equal velocity fringes in a Rayleigh-Bénard flow by a speckle method. *Appl. Opt.* 19: 1385–86

Meynart, R. 1982. Digital image processing for speckle flow velocimetry. *Rev. Sci. Instrum.* 53(1): 110–11

Meynart, R. 1983. Instantaneous velocity field measurements in unsteady gas flow by speckle velocimetry. *Appl. Opt.* 22(4): 535–40

Meynart, R. 1985. Non-Gaussian statistics of speckle noise of Young's fringes in speckle velocimetry. *Appl. Opt.* 24(10): 1448–53

Modares, D., Tan, H., Trollinger, J. D. 1985. Tomographic reconstruction of flow over air foils. *AIAA Pap. No. 85-0479*

Mohanty, R. K., Joenathan, C., Sirohi, R. S. 1984. Fringe sharpening and information coupling in speckle shear interferometry. *Appl. Opt.* 23(24): 4596–4600

Monorski, N. 1962. *Non-Linear Oscillators*. New York: Van Nostrand

Muller, R. K., Saackel, L. R. 1979. Complete automatic-analysis of photo-elastic fringes. *J. Exp. Mech.* 19: 245–51

Munk, W., Wunsch, C. 1979. Ocean acoustic tomography—a scheme for large scale monitoring. *Deep-Sea Res.* 26A: 123

Nakadate, S., Yatagai, T., Saito, H. 1983. Computer aided speckle pattern interferometry. *Appl. Opt.* 22: 237–43

Newman, W. M., Sproull, R. F. 1979. *Principles of Interactive Computer Graphics*. New York: McGraw-Hill

Olsen, H. N., Maldonado, C. D., Duckworth, G. D. 1968. A numerical method for obtaining internal emission coefficients from externally measured spectral intensities of asymmetrical plasma. *J. Quant. Spectrosc. Radiat. Transfer* 8: 1419–30

Oppenheim, A. V., Schafer, R. W. 1975. *Digital Signal Processing*. Englewood Cliffs, NJ: Prentice-Hall

Oppenheim, B. E. 1977. Reconstruction tomography in diagnostic radiology and nuclear medicine. In *Reconstruction Tomography from Incomplete Projections*, pp. 155–83. Baltimore, Md: University Park Press

Paek, E. G., Psaltis, D. 1987. Optical associative memory using Fourier transform holograms. *Opt. Eng.* 26(5): 428–33

Pavlidis, T. 1977. In *Structural Pattern Recognition*, pp. 222–26. Berlin: Springer-Verlag

Payne, P. R., Carder, K. L., Steward, R. G. 1984. Image analysis techniques for holograms of dynamic oceanic particles. *Appl. Opt.* 23(2): 204–10

Perkins, W. A., Laffey, T. J., Nguyen, T. J. 1986. Rule-based interpreting of aerial photographs using the Lockheed Expert System. *Opt. Eng.* 25(3): 356–62

Perry, A. E., Chong, M. S. 1987. A description of eddying motions and flow patterns using critical-point concepts. *Ann. Rev. Fluid Mech.* 19: 125–55

Pickering, C. J. D., Halliwell, N. A. 1984. Speckle photography in fluid flows: signal recovery with two-step processing. *Appl. Opt.* 23(8): 1128–29

Pickering, C. J. D., Halliwell, N. A. 1985. Particle image velocimetry: fringe visibility and pedestal removal. *Appl. Opt.* 24(16): 2474–76

Pratt, W. K. 1978. *Digital Image Processing.* New York: Wiley-Interscience

Prenel, J.-P., Porcar, R., Reiniche, S., Diemunsch, G. 1986. Visualizations tridimensionnelles d'écoulements non axisymétriques par balayage programmé d'un faisceau laser. *Opt. Commun.* 59(2): 92–96

Radon, J. 1917. Über die bestimmung von funktionen durch ihre integralwerte langs gewisser mannigfaltigkeiten. *Ber. Verh. Sächs. Akad. Wiss. Leipzig Math.-Phys. Kl.* 62: 262–77

Ray, S. R., Semerjian, H. G. 1983. Laser tomography for simultaneous concentration and temperature measurement in reacting flows. *Prog. Astronaut. Aeronaut.* 92: 300–24

Reid, G. T. 1986. Automatic fringe pattern analysis: a review. *Opt. Lasers Eng.* 7: 37–68

Rimai, L., Marko, K. A. 1982. Rapid digitized storage of seed-particle-track images in microscopically inhomogeneous flows. *Opt. Lett.* 7(7): 328–30

Rob, R. 1985. *Three-Dimensional Biomedical Imaging.* Boca Raton, Fla: CRC Press

Robinson, D. W. 1983. Automatic fringe analysis with a computer image-processing system. *Appl. Opt.* 22(14): 2169–76

Rowley, P. D. 1969. Quantitative interpretation of three-dimensional weakly refractive phase objects using holographic interferometry. *J. Opt. Soc. Am.* 59(11): 1496–98

Sakata, K., Shindoh, S., Yanagi, R. 1985. Experimental flow analysis with computer graphics on film cooling flow field. *Proc. Int. Symp. Flow Visualization, 3rd, 1983*, pp. 710–14. Washington, DC: Hemisphere

Santoro, R. J., Semerjian, H. G., Emmerman, P. J., Goulard, R. 1981. Optical tomography for flow field diagnostics. *Int. J. Heat Mass Transfer* 24: 1139–50

Schemm, J. B., Vest, C. M. 1983. Fringe pattern recognition and interpolation using nonlinear regression analysis. *Appl. Opt.* 22(18): 2850–53

Schon, J. P. 1984. Instantaneous concentration and velocity measurements through laser visualization associated with a digital processing system. In *Digital Image Processing in Fluid Mechanics.* Brussels: von Kármán Inst.

Schon, J. P. 1986. Instantaneous concentration and velocity measurements through laser visualization associated with a digital processing system. In *Digital Image Processing in Fluid Mechanics.* Brussels: von Kármán Inst.

Semerjian, H. G., Santoro, R. J., Goulard, R., Emmerman, P. J. 1981. Fluid mechanics of combustion systems. In *Optical Tomography for Diagnostics in Combusting Flows*, p. 109. New York: ASME

Serra, J. 1982. *Image Analysis and Mathematical Morphology.* New York: Academic

Shimizu, I., Yasuda, Y., Emori, Y. 1985. Quantitative visualization of jet sprays by a bi-directional light-scattering image processing method. *Proc. Int. Symp. Flow Visualization, 3rd, 1983*, pp. 358–64. Washington, DC: Hemisphere

Shtein, I. N. 1972. The use of the radon transform in holographic interferometry. *Radio Eng. Electron. Phys.* 17(11): 2436–37

Smith, R. E. Jr., Sperray, D. E., Everton, E. L. 1985. Visualization of computer-generated flow fields. *Proc. Int. Symp. Flow Visualization, 3rd, 1983*, pp. 655–62. Washington, DC: Hemisphere

Snyder, R., Hesselink, L. 1985. High speed tomography for flow visualization. *Appl. Opt.* 24: 4046–51

Snyder, R., Hesselink, L. 1984. Optical tomography for flow visualization of the density field around a revolving helicopter rotor blade. *Appl. Opt.* 23: 3650–56

Snyder, R., Hesselink, L. 1987. High speed optical tomographic data acquisition systems for combustion research. *Proc. Symp. Energy Eng. Sci., 5th.* In press

Sollid, J. E. 1975. Holography applied to structural components. *Opt. Eng.* 14: 460

Sommerscales, E. F. C. 1981. Fluid velocity by particle tracking. In *Flow, Its Measurement and Control in Science and Industry*, pp. 795–808. Research Triangle Park, NC: Ind. Inst. Am.

Stuck, B. W. 1977. A new proposal for estimating the spatial concentration of certain types of air pollutants. *J. Opt. Soc. Am.* 64: 668–78

Sweeney, D. W., Vest, C. M. 1973. Reconstruction of three-dimensional refractive index fields from multidirectional interferometric data. *Appl. Opt.* 12: 2649–64

Takeda, M., Ina, H., Kobayashi, S. 1982. Fourier-transform method of fringe-pattern analysis for computer-based topography and interferometry. *J. Opt. Soc. Am.* 72: 156–60

Thalmann, R., Dändliker, R. 1985a. High resolution video processing for holographic interferometry applied to contouring and measuring deformations.

Proc. Soc. Photo-Opt. Instrum. Eng. 492: 299–306

Thalmann, R., Dändliker, R. 1985b. Holographic contouring using electronic phase measurement. *Opt. Eng.* 24: 930–35

Toulouse, G., Hebrard, P., Lavergne, G., Calvet, P. 1985. Quantitative flow visualizations with video method and microcomputer. *Proc. Int. Symp. Flow Visualization, 3rd, 1983*, pp. 320–24. Washington, DC: Hemisphere

Toyooka, S., Iwaasa, Y., Kawahashi, M., Hosoi, K., Suzuki, M. 1985. Automatic processing of Young's fringes in speckle photography. *Opt. Lasers Eng.* 6: 203–12

Trolinger, J. D. 1985. Automated data reduction in holographic interferometry. *Opt. Eng.* 24: 840–42

Uberoi, M. S., Kovasznay, L. S. G. 1955. Analysis of turbulent density fluctuations by the shadow method. *J. Appl. Phys.* 26: 19–24

Uchiyama, H., Nakajima, M., Yuta, S. 1985. Measurement of flame temperature distribution by IR emission computed tomography. *Appl. Opt.* 24: 4111–16

Utami, T., Ueno, T. 1987. Experimental study on the coherent structure of turbulent open-channel flow using visualization and picture processing. *J. Fluid Mech.* 174: 399–440

Van Dyke, M. 1982. *An Album of Fluid Motion*. Stanford, Calif: Parabolic. 176 pp.

Vest, C. M. 1979. *Holographic Interferometry*. New York: Wiley. 465 pp.

Vest, C. M. 1974. Formation of images from projections: Radon and Abel transforms. *J. Opt. Soc. Am.* 64: 1215–18

Vest, C. M. 1975. Interferometry of strongly refracting axisymmetric phase objects. *Appl. Opt.* 14(7): 1601–6

Vest, C. M. 1985. Tomography for properties of materials that bend rays: a tutorial. *Appl. Opt.* 24: 4089–94

Willms, I. 1981. A measurement procedure for acquisition of spatial inhomogeneous aerosol concentrations. In *Aerosols in Science, Medicine, and Technology*

Winkelmann, A. E., Tsao, C. P. 1985. Flow visualization using computer-generated color video displays of flow field survey data. *Proc. Int. Symp. Flow Visualization, 3rd, 1983*, pp. 640–44. Washington, DC: Hemisphere

Wolf, E. 1969. Three-dimensional structure determination of semitransparent objects from holographic data. *Opt. Commun.* 1: 153–56

Wu, K., Hesselink, L. 1987. Application of depth cueing to computer display of reconstructed three-dimensional data. *Proc. IEEE.* In press

Watanabe, M., Seguchi, Y., Tomita, Y. 1979. Computer-aided fringe-pattern analyzer—a case of photoelastic fringe. *J. Exp. Mech.* 19: 362–70

Yamaguchi, I. 1984. Fringe formation in speckle photography. *J. Opt. Soc. Am. A* 1: 81–86

Yatagai, T., Idesawa, M. 1982. Automatic fringe analysis for Moire topography. *Opt. Lasers Eng.* 3: 73–83

Yatagai, T., Inaba, S., Nakano, H., Suzuki, M. 1984. Automatic flatness tester for very large scale integrated circuit wafers. *Opt. Eng.* 23: 401–5

Yip, B., Fourguette, D. C., Long, M. B. 1986. Three-dimensional gas concentration and gradient measurements in a photoacoustically perturbed jet. *Appl. Opt.* 25(21): 3919–23

Young, T. Y., Fu, K. S. 1986. *Handbook of Pattern Recognition and Image Processing*. New York: Academic

Zien, T.-R., Ragsdale, W. C., Spring, W. C. III. 1975. Quantitative determination of three-dimensional density field by holographic interferometry. *AIAA J.* 13(7): 841–42

Zimmermann, M., Miles, R. B. 1980. Hypersonic-helium-flow-field measurements with the resonant Doppler velocimeter. *Appl. Phys. Lett.* 37: 885–87